INTERNATIONAL JOURNAL OF AUTOMOTIVE AND MECHANICAL ENGINEERING
ISSN: 2229-8649 e-ISSN: 2180-1606
VOL. 21, ISSUE 4, 2024, 11784 – 11808
DOI: https://doi.org/10.15282/ijame.21.4.2024.5.0908

RESEARCH ARTICLE

Modelling, Simulation and Testing of Steer-by-Wire System with Variable Steering Ratio Control Strategy in 14-DOF Full Vehicle Model

M. A. Azizul[1,2], F. Ahmad[1]*, J. Karjanto[1], M. H. Che Hasan[3], and S. Sulaiman[2,4]

[1]Faculty of Mechanical Technology and Engineering, Universiti Teknikal Malaysia Melaka, 76100 Hang Tuah Jaya, Melaka, Malaysia
[2]Faculty of Engineering Technology, Universiti Tun Hussein Onn Malaysia, 84600 Panchor, Muar, Johor, Malaysia
[3]Faculty of Electric and Electronic Engineering Technology, Universiti Teknikal Malaysia Melaka, 76100 Hang Tuah Jaya, Melaka, Malaysia
[4]Vehicle Dynamic & Sustainable Development (VeDyS) Focus Group, Universiti Tun Hussein Onn Malaysia, 84600 Panchor, Muar, Johor, Malaysia

ABSTRACT – This research explores the application of Proportional-Integral-Derivative (PID) controllers and Variable Steering Ratio (VSR) control strategies within a Steer-by-Wire (SbW) system, utilizing a comprehensive 14 Degrees of Freedom (DOF) full vehicle dynamic model. The study aims to advance vehicle dynamics and control through SbW technology. This research addresses the challenge of optimizing steering control by integrating an SbW system with PID and VSR strategies to overcome the limitations of traditional steering mechanisms and enhance vehicle responsiveness and stability. The SbW system, using a PID-based controller, was rigorously tested and validated using MATLAB Simulink and Hardware-in-the-Loop System (HiLS) method. The performance of the system was assessed through four distinct signal tests: step, sine, square, and sawtooth inputs. These tests confirmed the precision of the PID controller in position tracking. To improve the practical applicability of the SbW system, a 14-DOF vehicle dynamic model was developed and validated before integration with the SbW system. The integrated system accurately replicated conventional steering behavior, as validated by Step Steer Input (SSI) and Double Lane Change (DLC) tests, demonstrating less than 11% RMS percentage error - well within the acceptable threshold of less than 15%. Additionally, the study proposed and validated VSR control strategies through the DLC test. Results indicate that the PID controller effectively tracked desired signals, while the VSR strategy reduced driver workload and improved steering stability. This research offers valuable insights into enhancing SbW system performance and lays a foundation for future advancements in vehicle control systems.

ARTICLE HISTORY
Received : 28th May 2024
Revised : 23rd Aug. 2024
Accepted : 22nd Sept. 2024
Published : 15th Nov. 2024

KEYWORDS
Steer-by-Wire
14 DOF vehicle model
Variable steering ratio
Control strategy
PID controller

1. INTRODUCTION

Vehicular control systems have advanced to new levels in pursuing automotive innovation. Among these, the Steer-by-Wire (SbW) technology stands out as a game changer by eliminating mechanical links between the steering system and tires. The integration of electric drivetrains with SbW technology surpasses the traditional model, encouraging an investigation into unexplored realms of vehicle management. This advancement in the steering system transmits the driver's steering commands from the mechanical system toward an electrical signal. By replacing the mechanical linkage with an electromechanical actuator, the SbW system offers better steering response performance. The absence of a mechanical shaft creates additional space, thereby enhancing the driver's safety and comfortability [1]–[2]. SbW system structure has two (2) major subsystems, known as the high module subsystem and low module subsystem, as shown in Figure 1. The high module's primary function is to receive any command from the user through the steering wheel by converting the driver's physical input to an electrical signal using the sensor positioned on the steering high module shaft. The low module control system also collects data from related sensors such as accelerometers, yaw rate, and gyro sensors to decide which priority orders need to be decided on and then sends it to the high module actuator. The low module's electric motor receives commands from the low module control system and attempts to regulate the low module angle accordingly. In the SbW system, road wheels are linked mechanically to the steering rack and the rack is further actuated by its corresponding motor. Thereby, the vehicle's responsiveness hinges on the movement of the steering rack. By leveraging the features of the SbW system, a tailored steering dynamic can be developed through the adjustment of control system parameters.

While the intelligent drive-by-wire system of electric vehicles offers advantages over conventional vehicles, it also faces core issues related to driving control [3]. Driving control, encompassing both lateral and longitudinal control, stands as a fundamental aspect in the dynamic research of electric vehicles. The steering system significantly impacts vehicle cornering stability and handling performance, as it primarily affects lateral dynamics [4]. Many studies have been conducted and diverse strategies have been recommended for the SbW steering systems based on different control approaches, such as conventional, recent, and robust control methods [5]. Drawing from the literature, several researchers have actively applied advanced control algorithms to develop SbW steering systems within simulation environments. These algorithms include Sliding Mode Control (SMC) [6]–[8], Neural Network Control (NNC) [9]–[11], Model

*CORRESPONDING AUTHOR | F. Ahmad | ✉ fauzi.ahmad@utem.edu.my

Predictive Control (MPC) [12]–[14], Iterative Learning Control (ILC) [15], Fuzzy Logic Control (FLC) [16]–[18], Linear Quadratic Gaussian Control (LQG) [19], Disturbance Observer Control (DOB) [20]–[21], and $H_2/H\infty$ control [22]–[23]. These applications aim to acquire, predict, and analyze various desired parameters of vehicle complex characteristics.

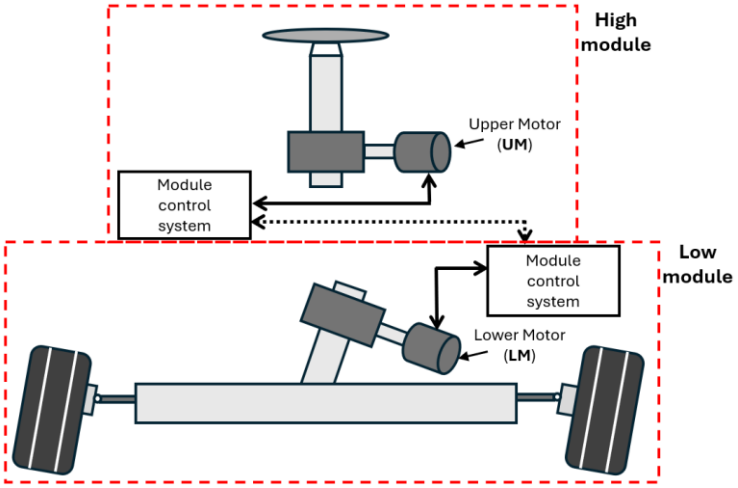

Figure 1. Structure of the SbW system

Despite significant contributions to SbW steering system development, the reliability of the results remains questionable due to challenges in the implementation process. This uncertainty arises because simulation studies on SbW steering system analysis typically involve low degree-of-freedom (DOF) of vehicle dynamic models, usually 2-DOF and 4-DOF. The simulation often fails to capture the full complexity of real-world dynamics, leading to discrepancies between simulated and actual performance. Analyzing the performance of SbW systems is crucial, and attention must initially focus on the simulation results to draw accurate conclusions before proceeding to experimental methods. Besides that, the advanced controllers introduced in the SbW system pose limited feasibility for implementation in microcontrollers. As mentioned in [24]–[26], the two degree-of-freedom (2-DOF) vehicle dynamic model is effective in grasping fundamental concepts related to vehicle dynamics, but it lacks the ability to accurately represent the impacts of suspension and tire characteristics. In other words, while the model may provide insights into how a vehicle behaves in response to steering inputs, acceleration, and braking, it does not account for the nuances introduced by the suspension system (which affects how the vehicle responds to bumps and uneven terrain) or the tire dynamics (which influence factors such as traction, grip, and handling). As a result, this model may not be sufficient for more detailed or realistic simulations where the effects of suspension and tire behavior are critical. Furthermore, although the advanced control system provides significant results and can be considered successful in a simulation environment, it is well recognized that those advanced controllers have drawbacks, such as complex iteration and models with additional non-linear influences in NNC [27], slow convergence rate that causes long time to achieve the desired level of performance in ILC [28], sensitivity to the tuning of the parameter in FLC [29], complex design and tuning in $H_2/H\infty$ control [30], chattering issue in SMC [31]–[33], complexity issue that lead slow control loop execution duration in MPC [34], and accuracy issue at high-frequency noise in DOB [35]. Thus, the potential of the advanced controller embedded in the SbW steering system cannot be fully exploited and verified.

Therefore, those advanced controllers raise doubts in terms of accuracy and ability to be implemented on real vehicles, that they need to be tested in real conditions. Besides that, a few researchers have successfully conducted limited experimental studies that yielded positive outcomes, mostly using the hardware-in-the-loop system (HiLS) method and the human-in-loop (HuL) method. HiLS is a hybrid simulation of software and hardware that is connected with each other to perform real-time dynamic simulation, especially for the introduction of advanced controllers that need more time to be implemented in the hardware system. As noted by Yang et al. [36], the validation of a HiL control system for a steering device was successfully conducted and provided significant results regarding the forecasting of steering wheel angle in the context of stimulating manual and driverless driving scenarios for active steering system application. However, limitations in the simulation system frequency and the computer's low performance affected the overall conduct of simulations using the HiL method. For the HuL method, known as the static driver simulator application, Alfatti et al. [37] investigated the efficacy of two advanced lateral stability controllers compared to a commercial solution. This assessment utilized a HiL simulation rig and a real-time static simulator involving various closed-loop maneuvers. The researchers aimed to boost stability performance by precisely tracking both yaw rate and side-slip angle using Sliding Mode Control (SMC) and Linear Quadratic Regulation (LQR) controllers, resulting in significant improvement. However, challenges arose in evaluating the performance of lateral stability controllers in vehicles where the yaw rate and the lateral acceleration are interrelated. The complexity stems from the intricate interaction among the vehicle, environment, and driver, which complicates the assessment of stability achievements. It can be inferred that those advanced controlllers greatly rely on parameter sensitivities and different vehicle constraints need to be considered when the vehicle model is embedded. These optimization algorithms face significant limitations when dealing with constraints and also require high computer performance to solve the constraint problem [23] that would lead the HiL/HuL approach stage to become costly.

Unlike proportional-integral-derivative (PID) controllers, known as classical controllers, which require uncomplex mathematical formulation. This controller offers simplicity through its straightforward formula, complete features, and automatic calculation of control signal output based on parameters entered that are integrated with the plant model. Additionally, PID control yields effective and improved results, particularly when tuned with adaptive algorithms [28]. In contrast to advanced controllers, PID controllers directly compare collected data values with reference data values, utilizing this error comparison to generate new inputs and minimize deviations, thereby maintaining system data values at the set point [38]. PID controller has also been extensively utilized in industrial applications due to its simplicity and ease of tuning. Furthermore, the PID controller has been applied to an electro-hydraulic steering system for a long time and has achieved a good control effect [39]. He et al. [40] introduced a new SbW system architecture, namely iSteer, aimed at achieving high-performance steering angle tracking for autonomous vehicles. Particle swarm optimization (PSO) has been used to fine-tune the parameters of an adaptive proportional-integral (PID) controller for real-time or embedded applications, emphasizing rapid and efficient computation. Experimental tests on a physical iSteer system validate the effectiveness of the architecture and the control law, showcase excellent accuracy of tracking ability and rapid response times for steering angle control in autonomous vehicles. Huang et al. [41] demonstrated two different types of control loops utilizing PID controllers to track trajectories in SbW systems with Coulomb friction to understand the essential differences between these control loops and the impact of the current loop on system performance. The results indicated that the performance exhibited by the two types of PID controllers, differing in arrangement of gain K_p, K_i, and K_d, successfully tracked trajectories with different response performances. The researchers assert that PID controllers remain widely used in engineering practice [42]–[44]. Thus, PID controllers were chosen and examined in real-time experiments. Phetnok et al. [45] have successfully modified an electric golf cart's steering system into steer-by-wire. It involves using a DC motor with a digital encoder controlled by an Arduino UNO microcontroller. PID controllers were employed and then implemented to control the feedback mechanism of the electric golf cart. The outcomes of this endeavor demonstrate commendable control performance in terms of path tracking and resisting disturbances. Additionally, this approach offers several advantages, including a reduction in time spent in tuning controller gains and a decrease in the likelihood of driver errors caused by repetition. Based on the literature, it can be determined that the proportional-integral-derivative (PID) controller offers a straightforward control strategy that is easy to develop and has a high potential for implementation in hardware systems for real-time experiments.

In the SbW system, the tires are not mechanically connected to the steering wheel, allowing for flexible adjustment of the steering ratio in various ways. At present, the steering ratio for conventional steering systems has been set between 1:15 and 1:22 ratio for passenger cars, and it is constant under all driving conditions. As a result, designing the steering ratio with a constant steering gain presents several challenges. For instance, at lower speeds, drivers generally anticipate a larger turning angle, so a small steering ratio might quickly bring the steering wheel to its maximum position. Conversely, as the vehicle accelerates, a constant yaw rate factor in the steering ratio could lead to increased steering sensitivity. On the other hand, employing a steering ratio based on a constant lateral acceleration factor may diminish the driver's sense of road feedback [46]. Thus, by implementing the variable steering ratio, a linear steering characteristic with a constant yaw rate factor can be established, enhancing maneuverability [4]. Many researchers have also explored and studied this area with various approaches. Yang et al. [47] proposed a new variable steering ratio (VSR) strategy that utilizes a fuzzy logic-based adaptive neural network along with a dynamic front steering controller to track the desired yaw rate. The proposed controller was embedded into a 2-DOF vehicle dynamic model and then validated through simulation tests and HiL experiments involving various driving scenarios conforming to ISO standards. The results demonstrated excellent handling stability and tracking performance by controller implementation. Wu and Li [4] proposed a new VSR characteristic for an SbW system aimed at enhancing vehicle handling performance based on input user at steering wheel and vehicle speed. The employment of the Takagi-Sugeno fuzzy neural network on steering ratio control was successfully developed into a 2-DOF vehicle model. The modelling results prove that the proposed system improves steering agility and enhances steering stability. However, the point to be noted here is most researchers did not take into account the overall dynamic analysis such as tire dynamic characteristics. Then, the reliability of the simulation-based studies remains uncertain due to their reliance on basic vehicle dynamic models and the complexities associated with implementing controllers in hardware systems. Thus, further research work is still needed.

This study explores the investigation of the SbW system that will be integrated with 14 degree-of-freedom (14-DOF) vehicle dynamic models for performance valuation, especially in path tracking capability. Besides that, to address the heavy steering effort at low speeds and the high lateral acceleration at high speeds, a novel variable steering ratio (VSR) control strategy is recommended. This study will show the efficacy of the VSR control strategy in improving both steering and vehicle dynamic performance. This paper is structured into six sections, beginning with an introduction, a review of relevant preliminary work, and an evaluation of the SbW steering system controller and previous research on VSR control strategy development. Section two introduces the development of mathematical equations for the comprehensive vehicle dynamic model, which consists of the ride model, handling model, weight transfer model, vehicle lateral and longitudinal tire slip angle model, tire dynamic model, and Pacejka tire model. This 14-DOF will be stimulated in MATLAB Simulink and followed by the validation stage in the third section. A detailed explanation of the modeling and simulation method of the SbW model, the validation process, and the introduction of PID-based control in the SbW model are presented in the fourth section. The fifth section presents an introduction of a new variable steering ratio (VSR) control strategy and the validation results of VSR in the full vehicle dynamic model. In this section, the capability of the PID controller and

VSR control strategies to track the trajectory and improvement of the vehicle's dynamic performance will also be presented. Lastly, the study provides the conclusions in the final section.

2. A 14-DOF VEHICLE DYNAMIC MODEL

To investigate the SbW system's capabilities for vehicle dynamic performances, a development of the mathematical model of the SbW system is required. A general study was conducted to select a model for the SbW system that will be integrated into the vehicle dynamic model and the selection of the SbW model will presented in Section 4.0. In this study, a 14-DOF vehicle dynamic model, also known as a comprehensive full vehicle dynamic model subjected to irregular road excitation, is considered. A full vehicle dynamic model was selected because this model provides a more realistic simulation of driving conditions [48]–[49]. This model can also replicate real-world scenarios, including varying road surfaces and driving behaviors, which are crucial for understanding vehicle dynamics in practical situations [50]. A full vehicle dynamic model is used to attain the dynamic yaw motion, pitch motion, roll motion, and non-linear effect stemming from vehicle geometry changes. The 14-DOF vehicle dynamics model includes the sprung mass of the vehicle body, which is represented by 6-DOF covering motion and rotational moments along the x, y, and z axes, as well as four unsprung masses for the tires, each with 2 DOF encompassing motion and rotational moments in the y-axis plane. The governing differential equations of motion for the full vehicle dynamic model can be directly derived from Lagrange's equations. Several assumptions have been made in this work, particularly that the vehicle body is modeled as rigid, which assumes that load transfer between points is one hundred percent effective. Additionally, it is assumed that the outer and inner steer angles are the same. During maneuvering, the vehicle suspensions springs will not be permitted to "top out". The aerodynamic impact on the vehicle is neglected, and it is assumed that the road is flat, with the exception of potential road disturbances. Throughout maneuvering, the vehicle maintains constant contact with the ground, ensuring that all four tires remain grounded. Additionally, the coefficient and stiffness parameters in the vehicle dynamic model are presumed to remain consistent throughout the simulation process [51]–[52].

2.1 Ride Model

The vehicle ride model, illustrated in Figure 2, is represented as a 7-DOF vehicle model. It features a sprung mass (vehicle body) coupled with four unsprung masses (tires, springs, and dampers) at each corner. The sprung mass body is permitted 3-DOF, including vertical, roll, and pitch motions.

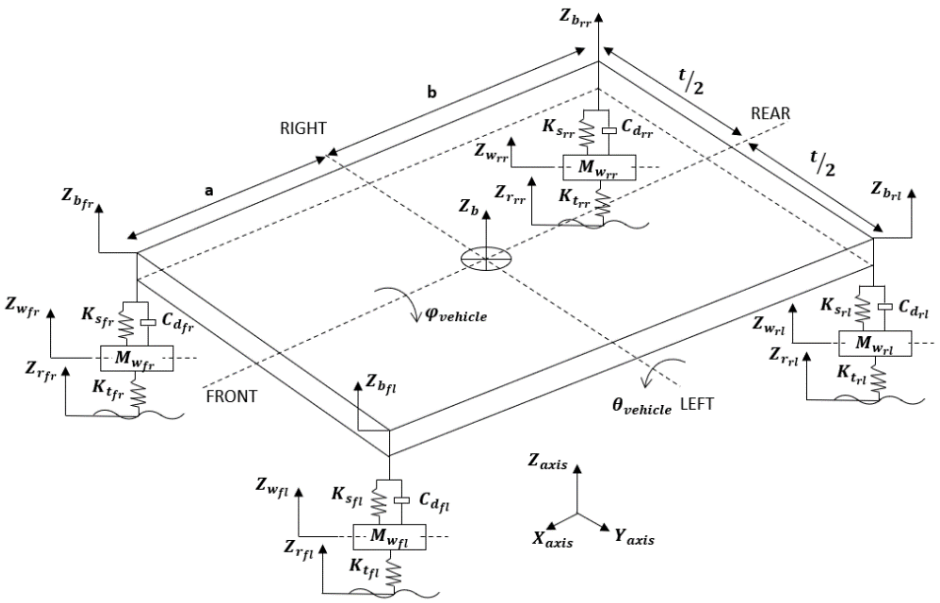

Figure 2. A 7-DOF vehicle ride model

By using Newton's Second law, the body's vertical acceleration, $\ddot{Z}_b$ can be formulated by:

$$M_b\ddot{Z}_b = F_{sfl} + F_{dfl} + F_{sfr} + F_{dfr} + F_{srl} + F_{drl} + F_{srr} + F_{drr} \quad (1)$$

where M_b is the mass of the vehicle, $F_{(s/d)\ fl/fr/rl/rr}$ represents the spring or damper force acting on the front left, front right, rear left and rear right of the tire, respectively.

The tire's vertical acceleration, $\ddot{Z}_w$can be determined by:

$$M_w\ddot{Z}_{w_{fl}} = F_{t_{fl}} - F_{s_{fl}} - F_{d_{fl}} \quad (2)$$

$$M_w\ddot{Z}_{w_{fr}} = F_{t_{fr}} - F_{s_{fr}} - F_{d_{fr}} \quad (3)$$

$$M_w \ddot{Z}_{w_{rl}} = F_{t_{rl}} - F_{s_{rl}} - F_{d_{rl}} \quad (4)$$

$$M_w \ddot{Z}_{w_{rr}} = F_{t_{rr}} - F_{s_{rr}} - F_{d_{rr}} \quad (5)$$

where M_w is the mass of the tire and F_t is the dynamic tire force. $F_{tfl/fr/rl/rr}$ represent the force acting on each of the tires. The spring force, F_{si} that acts on the suspensions at each of the tires is given by:

$$F_{si} = K_{si}(Z_{wi} - Z_{bi}) \quad (6)$$

where K_{si} is the suspension spring stiffness at each tire, Z_{wi} is the sprung mass of vertical displacement at each tire and Z_{bi} is the unsprung mass of vertical displacement at each tire. The damper force, F_{di} that act on the suspensions at each of the tire is given by:

$$F_{di} = C_{di}(\dot{Z}_{wi} - \dot{Z}_{bi}) \quad (7)$$

where C_{di} is the suspension damper coefficient at each tire, $\dot{Z}_{wi}$ is the sprung mass of vertical velocity at each tire and $\dot{Z}_{bi}$ is the unsprung mass of vertical velocity at each tire. The dynamic tire forces, F_{ti} is defined as:

$$F_{ti} = K_{ti}(Z_{ri} - Z_{wi}) \quad (8)$$

where K_{ti} is the spring stiffness of each tire, Z_{ri} is the road profile at each tire.

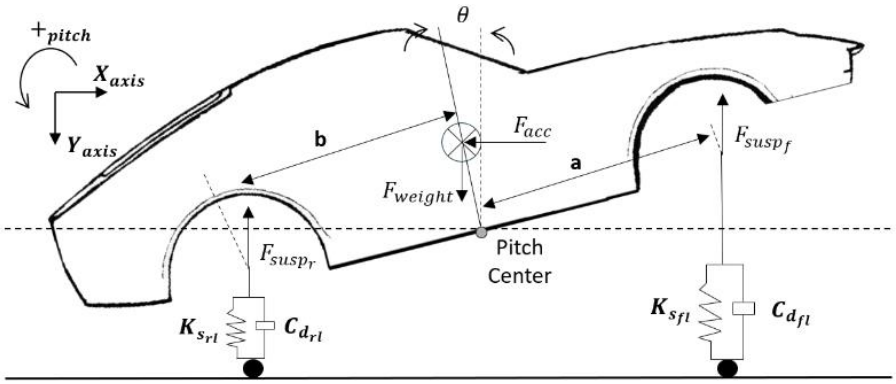

Figure 3. Free-body diagram for pitch motion

The pitch effect of the vehicle, illustrated in Figure 3 (free-body diagram of pitch motion), is given by:

$$I_\theta \ddot{\theta} = (F_{srl} + F_{drl} + F_{srr} + F_{drr})(b) - (F_{sfl} + F_{dfl} + F_{sfr} + F_{dfr})(a) \quad (9)$$

where I_θ represents the rotational inertia for the pitch axis, $\ddot{\theta}$ represents the pitch acceleration, θ represents the pitch angle, a and b represent the length from the center of vehicle gravity to the front end and the rear end of the vehicle.

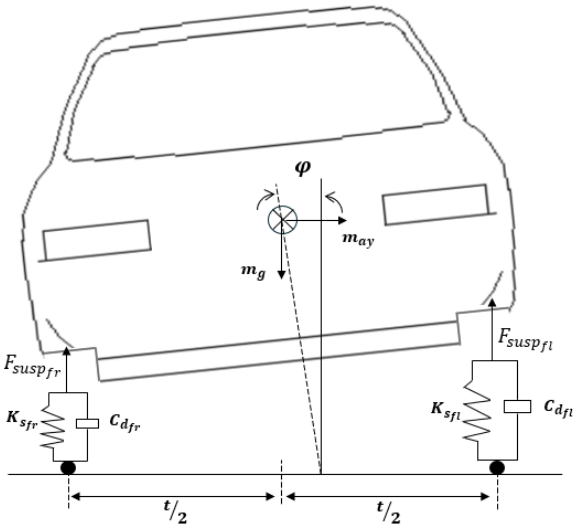

Figure 4. Free-body diagram for roll motion

The roll effect of the vehicle, shown in Figure 4 (free-body diagram for roll motion), is given by:

$$I_\varphi \ddot{\varphi} = (F_{sfl} + F_{dfl} + F_{srl} + F_{drl})(t/2) - (F_{sfr} + F_{dfr} + F_{srr} + F_{drr})(t/2) \quad (10)$$

where the I_φ is the rotational inertia for the roll axis, $\ddot{\varphi}$ is the roll acceleration, φ is the roll angle, t is the length of the wheel track.

2.2 Handling Model

The handling model presented in this research work incorporates a 3-DOF system to account for lateral, longitudinal, and yaw motions, with an additional 1-DOF component for the rotational motion of each tire. Figure 5 illustrates the model, depicting vehicle movement along the longitudinal and lateral directions as well as yaw rotation around the z-axis. The x-y plane motion is denoted by longitudinal and lateral accelerations, represented by a_x and a_y, respectively.

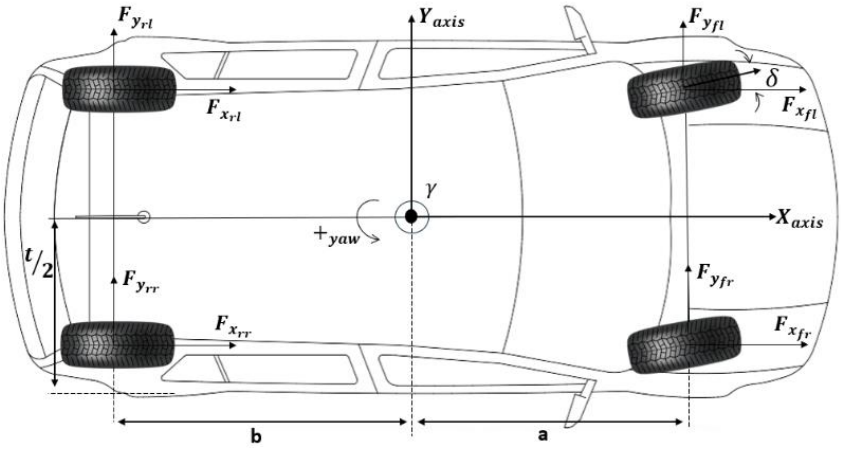

Figure 5. Free body diagram for handling motion

To determine the lateral and longitudinal accelerations, this model counts the total of all forces acting in both lateral and longitudinal directions. Total forces: the total longitudinal forces at the front and rear, which account for both normal and drag considerations, are expressed as follows:

$$F_{x_{total}} = F_{xfl}\cos\delta - F_{yfl}\sin\delta + F_{xfr}\cos\delta - F_{yfr}\sin\delta + F_{xrl} + F_{xrr} \tag{11}$$

$$F_{y_{total}} = F_{xfl}\sin\delta + F_{yfl}\cos\delta + F_{xfr}\sin\delta - F_{yfr}\cos\delta + F_{yrl} + F_{yrr} \tag{12}$$

The acceleration along the x-axis is represented as:

$$\dot{v}_x = a_x - v_y\gamma \tag{13}$$

The acceleration along the y-axis is represented as:

$$\dot{v}_y = a_y + v_x\gamma \tag{14}$$

The yaw motion relies on the forces exerted by each tire and is defined as:

$$\begin{aligned} I_\gamma\ddot{\gamma} = {} & (t/2)\{(F_{xfl}\cos\delta) + (F_{yfl}\sin\delta) + (F_{xfr}\cos\delta) + (F_{yfr}\sin\delta)\} + \\ & (a)\{((F_{xfl}\sin\delta) + (F_{yfl}\cos\delta) + (F_{xfr}\sin\delta) + F_{yfr}\cos\delta)\} + (b)\{F_{yrl} - F_{yrr}\} \end{aligned} \tag{15}$$

where δ is the wheel angle, $\dot{\gamma}$ is the yaw rate, γ is the yaw angle, I_γ is the rotational inertia for the yaw axis, v_y is the lateral vehicle velocity and v_x is the longitudinal vehicle velocity.

2.3 Weight Transfer Model

The weight transfer model is based on lateral and longitudinal acceleration due to inertia. In this study, dynamic weight transfer is shifted between left and right wheels during maneuvers such as cornering conditions. Meanwhile, the distribution of load between the front and rear wheels changes during acceleration, braking and cornering. This formula is derived under specific assumptions, including the exclusion of suspension dynamics and the disregard of roll and pitch coupling effects.

From the geometry based on Figure 6, normal forces for front and rear tires can be formulated as:

$$F_{z,fl/fr} = \left(\frac{mgb - H_{CG}ma_x}{2(l)}\right) \tag{16}$$

$$F_{z,rl/rr} = \left(\frac{H_{CG}ma_x}{2(l)}\right) + \left(\frac{mga}{2(l)}\right) \tag{17}$$

where H_{CG} is the length from the center of gravity to the bottom of the vehicle and l is the total summation of a and b known as the vehicle's wheelbase. At the same time, θ represents the road incline. For the purposes of this study, the road surface is considered to be flat (0°) for all standard tests.

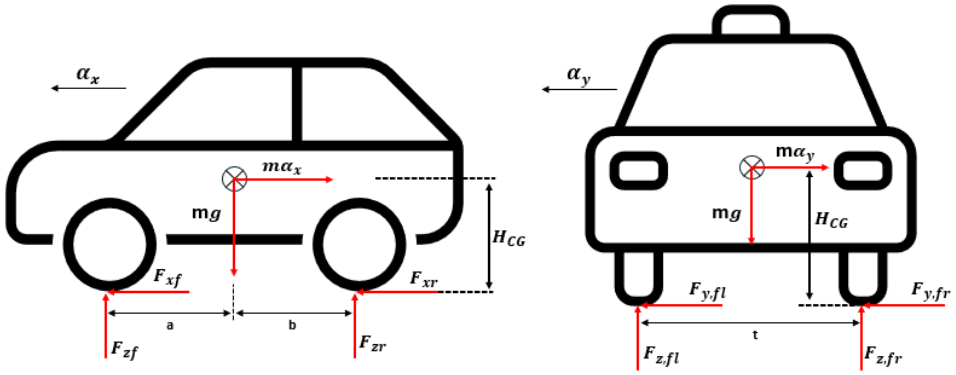

(a) (b)

Figure 6. Weight transfer during (a) acceleration and (b) cornering

2.4 Vehicle Lateral and Longitudinal Tire Slip Angle Model

The lateral and longitudinal vehicle velocities, denoted as v_x and v_y can be obtained by integrating the accelerations $\dot{v_x}$ and $\dot{v_y}$, respectively, as given in equations (13) and (14). This can be employed to determine the tire's lateral slip angle, represented by α. Therefore, the lateral slip angles for all sides of the tire can be determined as follows:

$$\alpha_{fl/fr} = \tan^{-1}\left[\frac{v_y + I_f\dot{r}}{v_x + \left(\frac{t}{2}\right)\dot{r}}\right] - \delta_f \tag{18}$$

$$\alpha_{rl/rr} = \tan^{-1}\left[\frac{v_y - I_r\dot{r}}{v_x + \left(\frac{t}{2}\right)\dot{r}}\right] \tag{19}$$

The side slip angle, denoted by β, can be formulated from the vehicle's body speed, as demonstrated in the following equation:

$$\beta = \tan^{-1}\left[\frac{v_y}{v_x}\right] \tag{20}$$

For the longitudinal tire slip angle formula, the longitudinal velocity component on both sides of the tire (front and rear) needs to be determined. The velocity of the front tire can be determined as follows:

$$v_f = \sqrt{\left(v_y - a.\dot{\gamma}\right)^2 + {v_x}^2} \tag{21}$$

Thus, the longitudinal velocity component of the front tire can be formulated as:

$$v_{xf} = v_f \cos\alpha_f \tag{22}$$

The velocity of the rear wheel is presented below:

$$v_r = \sqrt{\left(v_y + b.\dot{\gamma}\right)^2 + {v_x}^2} \tag{23}$$

Then, the longitudinal velocity component of the rear wheel can be determined as follows:

$$v_{xr} = v_r \cos\alpha_r \tag{24}$$

Next, the longitudinal slip ratio of the front and rear tire can be represented as:

$$\sigma_{f/r} = \frac{\left(v_{f/r} - \omega_{f/r}R_w\right)}{\max\left(v_{xf/r}\,,\ \omega_{f/r}R_w\right)} \tag{25}$$

where $\omega_{f/r}$ is the angular velocity of the front or rear tire and R_w is the tire radius.

2.5 Tire Dynamic Model

Throttling and braking torques are acting on the tire, along with the torque exerted by the viscous forces.

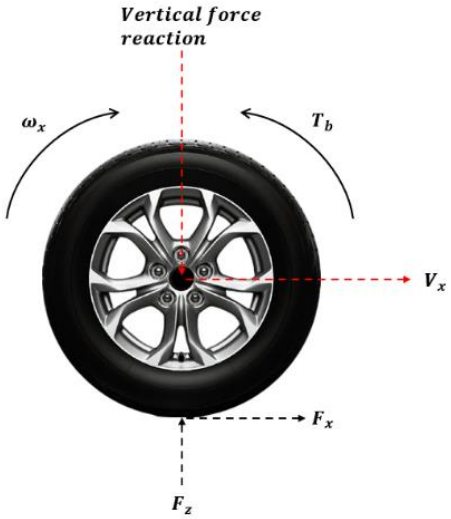

Figure 7. Free-body diagram for tire motion

For front and rear tires, the total torque about the axis, as illustrated in Figure 7 (free-body diagram for tire motion) are formulated as:

$$I_\omega \ddot{\omega}_{fl} = T_{dfl} - T_{bfl} - T_{trac.fl} \quad (26)$$

$$I_\omega \ddot{\omega}_{fr} = T_{dfr} - T_{bfr} - T_{trac.fr} \quad (27)$$

$$I_\omega \ddot{\omega}_{rl} = -(T_{brl} + T_{trac.rl}) \quad (28)$$

$$I_\omega \ddot{\omega}_{rr} = -(T_{brr} + T_{trac.rr}) \quad (29)$$

where,

$$T_{trac.} = F_x(R_w) \quad (30)$$

$$F_x = \mu(F_z) \quad (31)$$

$$F_z = -M_w g \quad (32)$$

where, μ is the coefficient friction of the road, I_ω is the inertia of the tire on the axle, T_d is driving torque, T_b is the applied braking torque, and $T_{trac.}$ is the traction torque.

2.6 Pacejka Tire Model

The tire model used in this work is the Pacejka tire model (known as the "Magic Formula" tire model) as proposed by Bakker et. al. [53] in 1987. This model was developed without a specific physical basis and through the integration of various tire characteristics and operational scenarios [54]. The Pacejka tire model has the capability to consider combined slip conditions where both the longitudinal slip and slip angle exist at the same time [55]–[56]. This model accurately represents tire mechanics based on real experimental test data, and the common equation for this model is provided in equation (33).

$$F(x) = D\cos\left(C\tan^{-1}\left(Bx - E(Bx - \tan^{-1}(Bx))\right)\right) \quad (33)$$

In the Magic Formula tire model, $F(x)$ and $F(y)$ represent the forces affecting tire lateral and longitudinal dynamics, respectively. The formula can use either the longitudinal slip, k or the lateral slip, α as parameters to determine whether it represents the impact on lateral or longitudinal forces [57]. To determine the lateral force, it can be computed using the following equations:

$$BCD = a_3 \sin(a_4 \tan^{-1}(a_5 F_z)) \quad (34)$$

$$B = BCD/CD \quad (35)$$

$$D = a_1 F_z^2 + a_2 F_z \quad (36)$$

$$C = 1.30\ (constant\ value) \quad (37)$$

$$E = a_6 F_z^2 + a_7 F_z + a_8 \quad (38)$$

The factors are minimally influenced by the camber angle, denoted as ϑ_c, measured in degrees,

$$S_h = a_9 \vartheta_c \quad (39)$$

$$S_v = (a_{10}F_z^2 + a_{11}F_z)\vartheta_c \quad (40)$$

To calculate the self-aligning moment and longitudinal force, it can be evaluated as detailed below:

$$BCD = (a_3F_z^2 + a_4F_z)/e^{a_5F_z} \quad (41)$$

$$B = BCD/CD \quad (42)$$

$$C = 2.40 \text{ / } 1.65 \ (constant\ value) \quad (43)$$

$$D = a_1F_z^2 + a_2F_z \quad (44)$$

$$E = a_6F_z^2 + a_7F_z + a_8 \quad (45)$$

where,

C = 2.40, constant for self-aligning moment.
C = 1.65, constant for longitudinal force.

The a parameter for the tire studied by Bakker et al. [53] is quoted in Table 1.

Table 1. The coefficient for tire formula

	a_1	a_2	a_3	a_4	a_5	a_6	a_7
$F_{(y)}$	-22.100	1011.000	1078.000	1.820	0.208	0.000	-0.354
$M_{(z)}$	-2.720	-2.280	-1.860	-2.730	0.110	-0.070	0.0643
$F_{(x)}$	-21.300	1144.000	49.600	226.000	0.069	-0.006	0.0560

	a_8	a_9	a_{10}	a_{11}	a_{12}	a_{13}
$F_{(y)}$	0.707	0.028	0.000	14.800	0.022	0.000
$M_{(z)}$	-4.040	0.015	-0.066	0.945	0.030	0.070
$F_{(x)}$	0.486	-	-	-	-	-

3. VALIDATION OF 14-DOF VEHICLE DYNAMIC MODEL

A verification simulation has been developed for the 14-DOF vehicle dynamic model by comparing the results from MATLAB Simulink and CarSim software. The 14-DOF vehicle dynamic model was created based on the mathematical formulations derived in Section 2.1 to Section 2.6. The correlation between the ride model, handling model, the Pacejka tire model, longitudinal and lateral slip model, and slip angle model are shown in Figure 8. To perform dynamic analysis for this model, four (4) inputs were utilized, namely steering input, throttle input, longitudinal velocity, and road profile. The validation test for the 14-DOF vehicle model is conducted by implementing different testing scenarios based on the International Organization for Standardization (ISO). In this work, two (2) tests were conducted, namely the Double Lane Change (DLC) test (ISO3888) and the Step Steer Input (SSI) test (ISO7401). SSI test is a vehicle dynamic test that evaluates the handling characteristic of a vehicle and is typically conducted in the low to middle vehicle speed category [58]. DLC test is the test to assess the vehicle's dynamic stability and performance in emergency situations [59]–[60]. DLC test typically is handled in the middle to high vehicle speed category. In this validation section, the SSI test was carried out with a 180° step steer at 60 km/h, while the DLC test was carried out at a constant speed of 80 km/h.

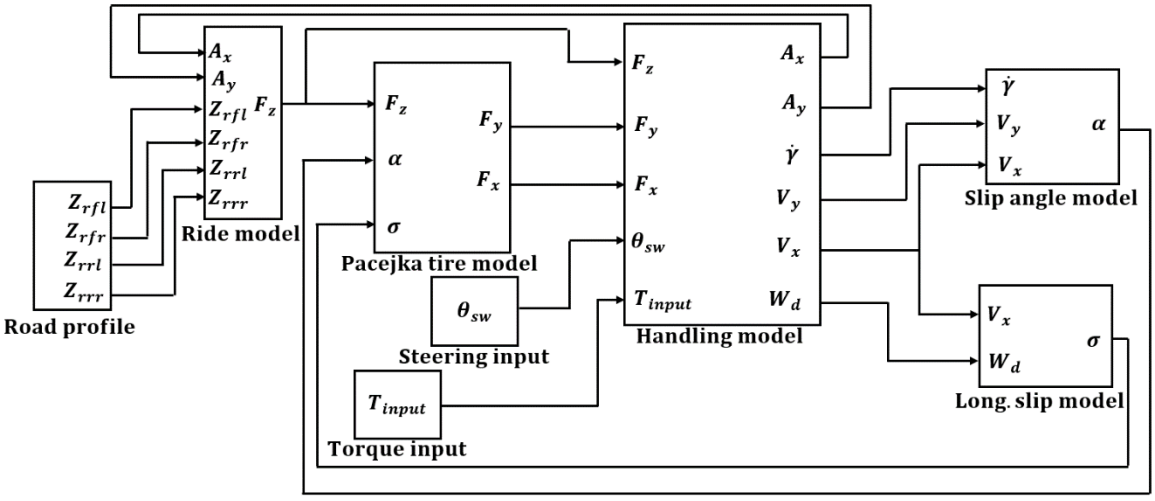

Figure 8. 14-DOF vehicle dynamic model in MATLAB Simulink

The parameters of the vehicle model used in MATLAB Simulink are shown in Table 2, sourced from CarSim software. The 2017 Hatchback, from the A-class vehicle chassis type parameter, was selected in the validation stage, as presented in Figure 9.

Figure 9. Vehicle model based on Hatchback A-class type. (Source: CarSim software)

Table 2. Parameter of vehicle model from CarSim software

Parameter	Symbol	Value	Parameter	Symbol	Value
Mass of vehicle	m	833 kg	Suspension spring stiffness front	K_{sf}	18000 N/m
Track width	t	1.415 m	Suspension spring stiffness rear	K_{sr}	18000 N/m
Wheelbase	l	2.35 m	Distance from ground to CG	H	0.54 m
Distance front axle to CG	a	1.1 m	Moment of roll	I_{φ}	270 kgm^2
Distance rear axle to CG	b	1.25 m	Moment of pitch	I_{θ}	750 kgm^2
Suspension damping constant front	C_{df}	1.032	Moment of yaw	I_{γ}	750 kgm^2
Suspension damping constant rear	C_{dr}	1.032	Tire radius	R_w	0.27 m
Frontal area of vehicle	A	1.6 m^3	Gravitational acceleration	g	9.81 m^2
Mass of wheel	M_w	20.75 kg			

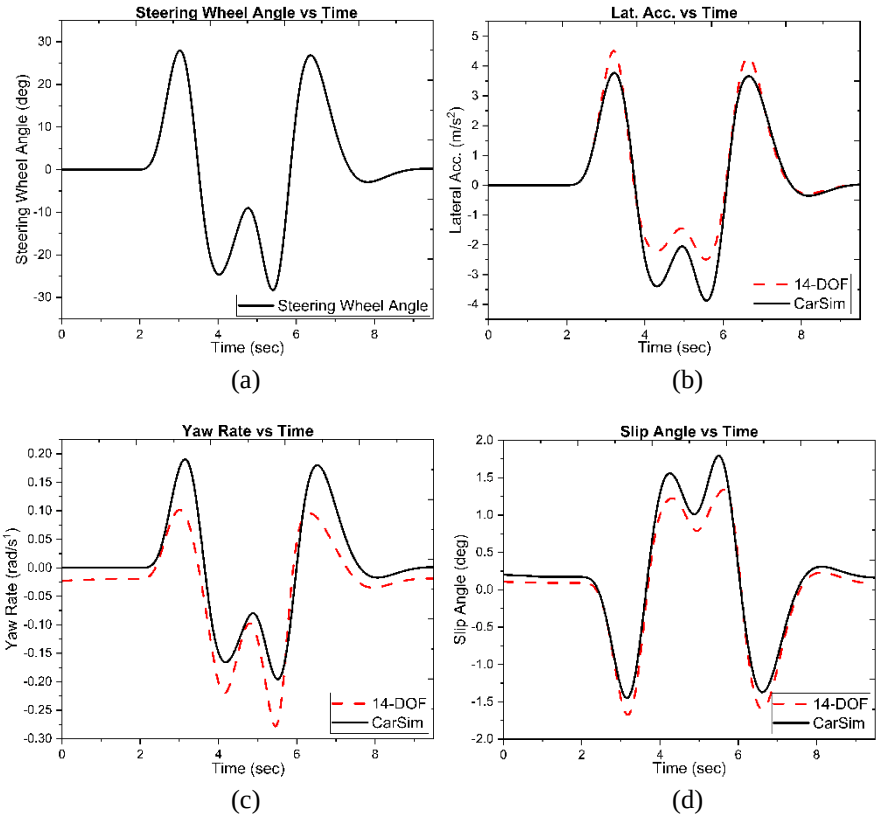

Figure 10. Vehicle dynamic characteristics for DLC test; (a) Steering wheel angle, (b) Lateral acceleration, (c) Yaw rate and (d) Slip angle of the front left tire

Figures 10(a) and 11(a) illustrate the steering inputs used for each test, with data sourced from CarSim software. The 14-DOF vehicle dynamic model was validated in terms of lateral acceleration, yaw rate, and tire slip angle. The validation process began with the DLC test, followed by the SSI test. Figures 10(b) through 10(d) present a comparison of the results between the CarSim and the MATLAB Simulink vehicle model output for the DLC test. The trends observed in the simulations align closely with the CarSim data, though there are minor differences in magnitude. The results were assessed by comparing the error percentage of root mean square (RMS) value from both software packages, where CarSim output serves as the benchmark. As per the guidelines reported by Udas. [61], Toffin et. al. [62] and Aparow et. al. [56], an acceptable range for RMS error percentage in model verification is between 0% and 15%. The RMS error percentage observed were 8.3% for lateral acceleration, 9.7% for yaw rate, and 6.1% for tire slip angle, all of which fall within the acceptable range of less than 15%. This error may be caused by the simplified model used in Simulink and the different numerical solvers or settings used between MATLAB Simulink and CarSim software. Besides that, a model from CarSim software was developed based on the actual tested vehicle simulation process; thus, it is better for precision. Furthermore, the differences could be due to variations in the underlying assumptions and parameterizations used in each software, as CarSim may incorporate more detailed and specific vehicle dynamics and road interaction models, while Simulink's models might rely on more generalized assumptions.

The SSI test results at 60 km/h show that the simulation outcomes are in reasonable agreement with the CarSim data. The plotted data indicates that the simulation model results are consistent with the CarSim data patterns, similar to those observed in the DLC test results, although there are some minor differences in magnitude, as illustrated in Figure 11(b) to Figure 11(d). Based on the results, the RMS error percentage for lateral acceleration is 10.5%, the yaw rate is 6.1%, and the slip angle is 2.7%, respectively, where all the errors are less than 15%. From both test results, it has been proven that the 14-DOF vehicle dynamic model that has been developed can be used to represent an actual vehicle dynamic model behavior for this work.

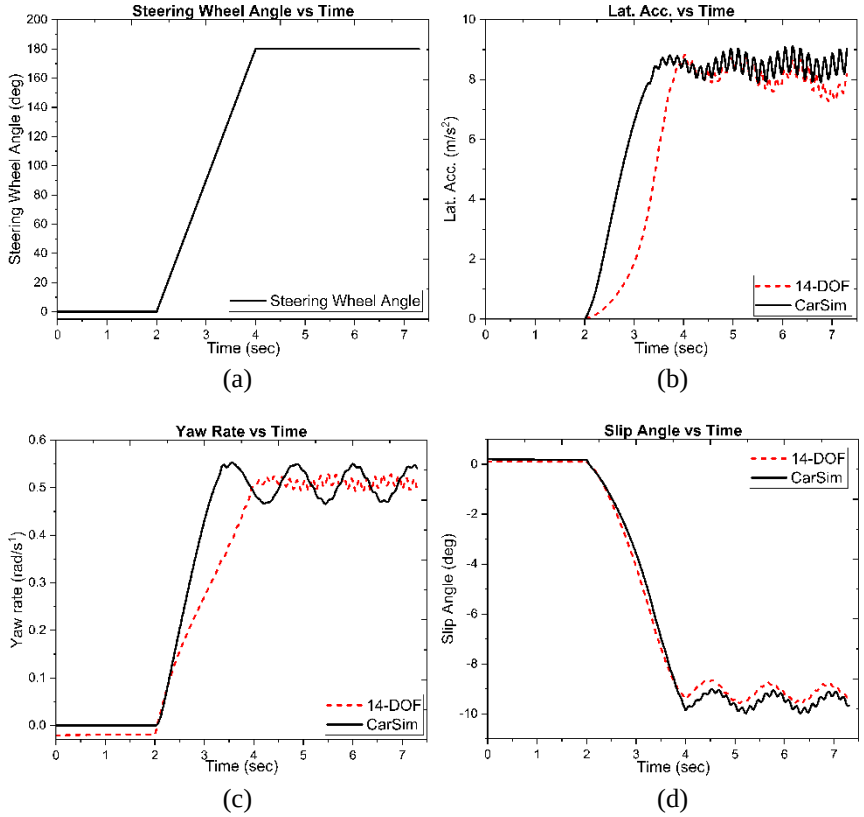

Figure 11. Vehicle dynamic characteristics for SSI test; (a) Steering wheel angle, (b) Lateral acceleration, (c) Yaw rate and (d) Slip angle of the front left tire

4. MODELLING AND VALIDATION OF STEER-BY-WIRE DYNAMIC MODEL

The SbW system can be categorized into two (2) subsystems, one representing the user system (known as the steering wheel subsystem), while the other representing the road system (known as the front wheel subsystem) [63]. The fundamental structure of the SbW system has been mentioned in Section 1.0, while the dynamic equation for the steering wheel, electric actuator, rack and wheel angular displacement are shown in Section 4.1 and Section 4.2. The SbW model was then developed in MATLAB Simulink, and the dynamic performance was compared with the data provided by CarSim software. The validation process is presented in Section 4.3 and Section 4.4.

4.1 Steering Wheel Model

The steering system assembly was mathematically modeled using Newton's laws to derive the dynamic formulation for wheel angle displacement relative to the kingpin axis. The primary external input to the steering system is the driver input torque, T_{driver}, applied at the steering wheel, while the wheel rotational angles represent the intended outputs. Positioned at the steering wheel, a DC motor aids the driver's input by converting their movements into electric signals. This specific DC motor located at the steering wheel is referred to as "Motor 1".

The corresponding systems diagrams for the steering wheel model are illustrated in Figure 12(a). Based on Newton's laws of motion and disregarding the transmission ratio between motor 1 and the steering wheel [64], the dynamic equation of the steering wheel assembly model can be defined as:

$$I_{sw}\ddot{\theta}_{sw} = \left(T_{driver} - B_{sc}\left(\dot{\theta}_{sw} - \dot{\theta}_{m1}\right) - K_{S1}(\theta_{sw} - \theta_{m1}) - T_{fr,c}\right) \tag{46}$$

where I_{sw} is the equivalent moment of inertia of the steering wheel, B_{sc} is the viscous damping of the steering wheel, K_{S1} is the lumped short-column compliance, $T_{fr,c}$ is the equivalent torque friction of the steering wheel and T_{driver} is the torque input from the driver. The upper motor equation of motion can be established as:

$$I_{m1}\ddot{\theta}_{m1} = \left(T_{m1} - B_{m1}\dot{\theta}_{m1} - B_{sc}\left(\dot{\theta}_{m1} - \dot{\theta}_{sw}\right) - K_{S1}(\theta_{m1} - \theta_{sw})\right) \tag{47}$$

where I_{m1} is the rotational inertia of the shaft motor 1, T_{m1} is the torque motor 1, θ_{sw} and $\dot{\theta}_{sw}$ are the steering wheel's angular displacement and angular velocity, B_{m1} is the viscous damping of the shaft motor 1, θ_{m1} and $\dot{\theta}_{m1}$ are the angular displacement and angular velocity of motor 1. For the steering wheel DC motor current formula, it can be defined from equations (48) and (49) based on Kirchhoff Voltage Law (KVL) and the diagram of the motor circuit can be referred to Figure 12(b). The overall steering DC motor formula is defined as follows:

$$V_{S1} = \left(V_{inductor} + V_{motor\ resistance} + V_{emf}\right) \tag{48}$$

$$= \left(\frac{di_{a1}}{dt}L_1 + R_1 i_{a1} + k_e\dot{\theta}_{m1}\right) \tag{49}$$

where V_{S1} is the voltage source to motor 1, $V_{inductor}$ is the voltage across the inductor formulated from Faraday's Law, $V_{motor\ resistance}$ is the voltage across the motor resistance formulated from Ohm's Law, V_{emf} is the electromotive force (emf) voltage applied to the motor, L_1 is the inductance of motor 1, R_1 is the resistance of motor 1, k_e is the electromotive force constant, and i_{a1} is the current of motor 1.

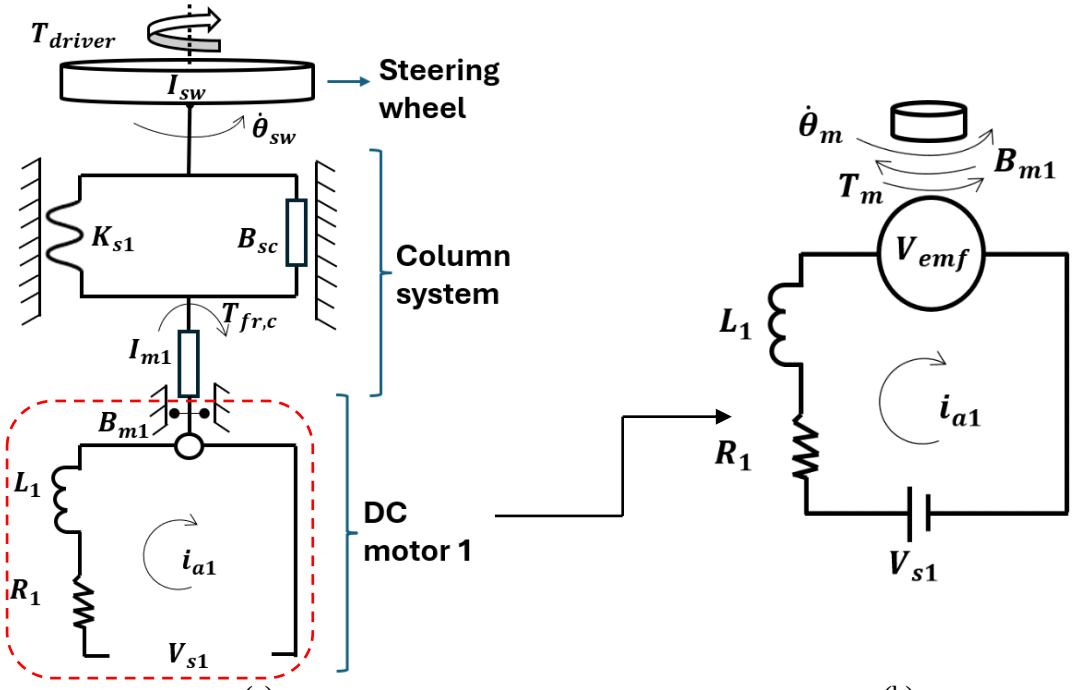

Figure 12. Free body diagram; (a) Steering wheel model, (b) Circuit model of the DC motor

4.2 Front Wheel Model

Figure 13 shows the diagram for the front wheel model. To formulate the front wheel model, the equations for rack bar displacement, vehicle tire deflection, and front wheel motor are required. DC motor is located at the rack, and the pinion assembly directly controls the movement of the wheel. The motor adjusts the position of the rack, which in turn

moves the wheels accordingly, allowing for precise and responsive steering control. This specific motor located at the front wheel system is referred to as "Motor 2". Its free body diagram is indicated by a red circle in Figure 13, while the circuit model of the front wheel DC motor 2 matches Diagram (12(b)).

Equations (50), (51), and (52) represent the front wheel modeling.

$$\ddot{y}_{rack_y} = \frac{1}{M_{rack}}\left(-\frac{2K_{Lf}}{r_L}\left(\frac{y_{rack_f}}{r_L}-\delta_F\right)-F_{fr,rack_f}-B_{rack_f}\dot{y}_{rack_f}+\frac{K_{s2}}{r_P}\left(\theta_{m2}-\frac{y_{rack_f}}{r_P}\right)\right) \quad (50)$$

$$\ddot{\delta}_F = \frac{1}{I_f}\left(-K_{Lf}\left(\delta_F-\frac{y_{rack_f}}{r_L}\right)-T_{fr,kpf}-B_{kpf}\dot{\delta}_F-M_z\right) \quad (51)$$

$$I_{m2}\ddot{\theta}_{m2} = \left(T_{m2}-B_{m2}\dot{\theta}_{m2}-K_{S2}\left(\theta_{m2}-\frac{y_{rack_f}}{r_P}\right)\right) \quad (52)$$

where M_{rack} is the mass of the rack, y_{rack_f} is the lateral displacement of the rack, $\dot{y}_{rack_f}$ is the lateral velocity of the rack, K_{Lf} is the steering linkage stiffness, K_{s2} is the lumped torque sensor stiffness, r_L is the offset of the king pin axis at applied force, r_P is the pinion gear radius, $F_{fr,rack_f}$ is the rack friction, B_{rack_f} is the damping coefficient of the rack, $T_{fr,kpf}$ represents the friction torque around the king pin axis, I_f is the rotational inertia of the wheel, I_{m2} is the rotational inertia of the shaft motor 2, M_z is the wheel aligning moment, B_{m2} is the viscous damping of the shaft motor 2, T_{m2} is the torque motor 2, θ_{m2} and $\dot{\theta}_{m2}$ are the angular displacement and angular velocity of motor 2, δ_F and $\ddot{\delta}_F$ are the actual front wheel steer angle and front wheel angular velocity, respectively. The formula for the front wheel DC motor of motor 2 can be expressed using the same equations as (48) and (49).

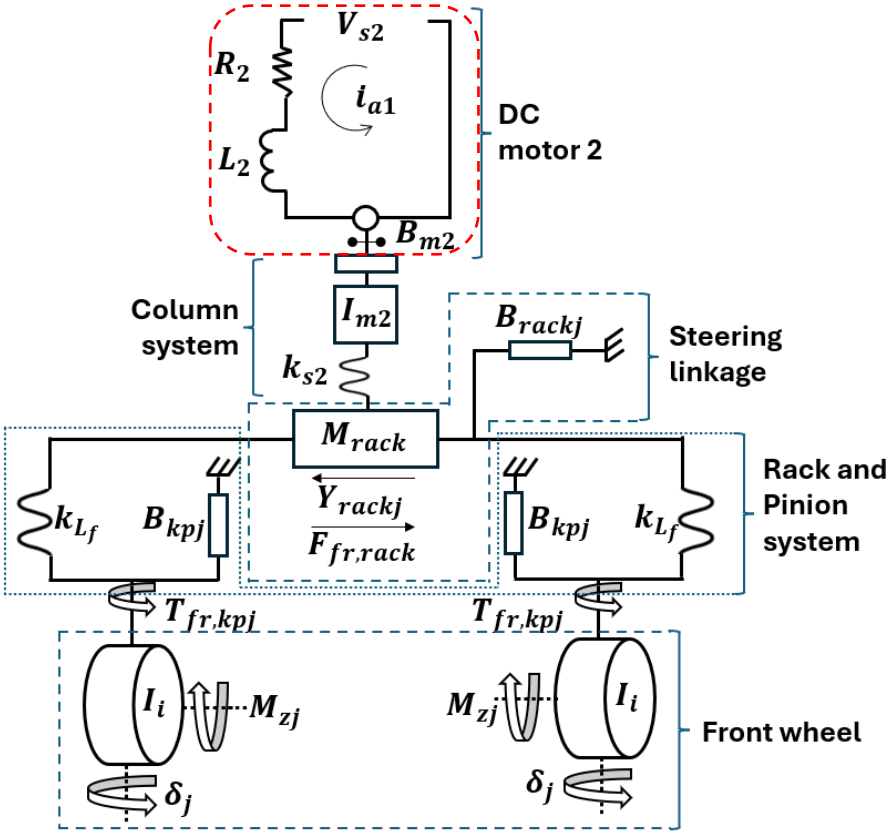

Figure 13. Free body diagram for front wheel model in SbW system

4.3 Position Tracking Steering Wheel Model in SbW system

Upon establishing all main vehicle subsystems, the SbW steering model was developed in Matlab Simulink and the tracking trajectory performance result was verified using data from CarSim software. The purpose of this validation is to attain a confident level of model accuracy before proceeding to real-world experiments. The parameters for the SbW model used in the validation process are provided in Table 3 and Table 4.

Table 3. Steering wheel model parameters

Parameter	Symbol	Value	Parameter	Symbol	Value
Motor 1 resistance	R_1	4.6 ohm	Offset of king pin axis	K_{sf}	18000 N/m
Motor 1 inductance	L_1	0.002 H	Motor emf constant	K_e	0.35 Vs/rad
Motor inertia	I_{sc}	1 kgm^2	Steering column damping	B_{sc}	0.136 Nms/rad
Motor damping	B_{m1}	1 Nms/rad	Lumped torque stiffness	K_{s1}	0.025 Nm
Lumped torque stiffness	K_{sc}	3500 Nm/rad	lumped short column compliance	T_{fr}	2 Nm

Table 4. Front wheel model parameters

Parameter	Symbol	Value	Parameter	Symbol	Value
Motor 2 resistance	R_2	0.6 ohm	Offset of king pin axis	r_L	0.3 m
Friction torque about king pin axis	$T_{fr,kpf}$	2 Nm	Rack friction	$F_{fr,rackf}$	9 Nm
Motor 2 inductance	L_2	0.002 H	Pinion gear radius	r_P	0.035 m
Motor 2 damping	B_{m2}	1 Nms/rad	King pin damping coefficient	B_{kpf}	30 Nms/rad
Lumped torque stiffness	K_{m2}	3500 Nm/rad	Lumped front wheel inertia	I_f	270 kgm^2
Rack damping coefficient	B_{rack}	1.032 Nms/rad	Motor 2 torque stiffness	K_{m2}	750 kgm^2
Rack lumped mass	M_{rack}	2.0 kg	Motor 2 inertia	I_{m2}	1.9 kgm^2
Steering linkage stiffness	K_{Lf}	26000 Nms/rad	Lumped torque sensor stiffness	K_{s2}	3500 Nm/rad

According to the dynamic equation of the steering wheel and front wheel model from equation (46) to (49), the block diagram was designed in MATLAB Simulink and shown in Figure 14. In this development, the proportional-integral-derivative (PID) controller was introduced in both models to enhance the transient response and tracking capability of the SbW model.

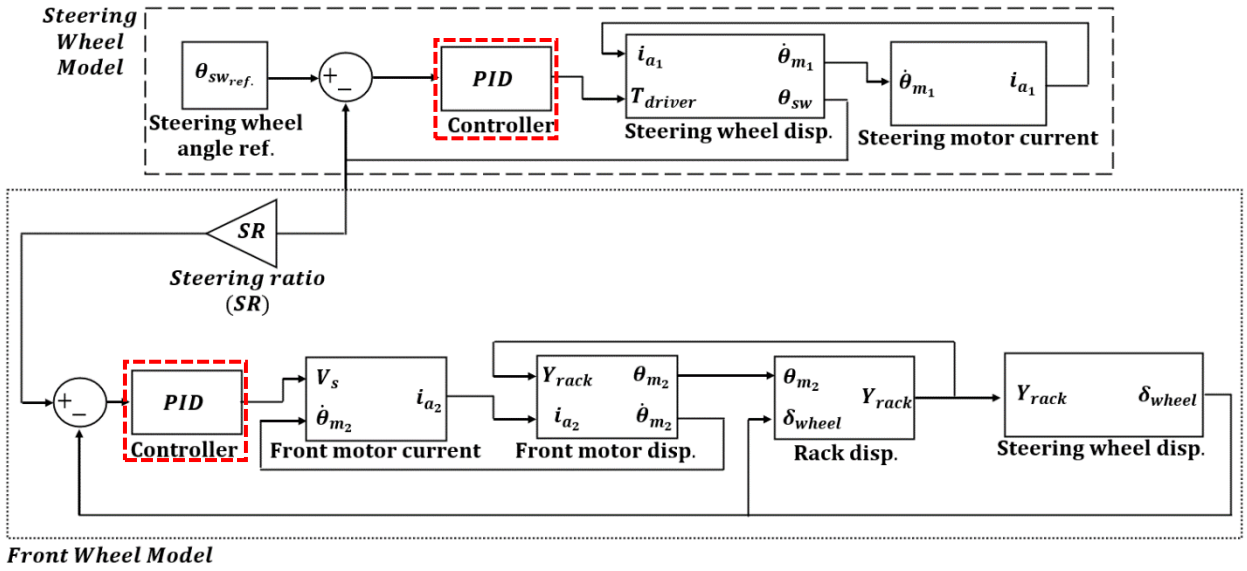

Figure 14. SbW model in MATLAB Simulink

In order to verify the validity of the SbW model, four (4) signal inputs were applied to the steering wheel input in both the simulation environment and the Hardware-In-the-Loops System (HiLS). To line up a HiLS, a complete SbW test rig is set up first, as shown in Figure 15 for the validation experiment. This test rig comprises various components, including a hardware processor serving as an ECU to regulate the SbW system, DC motor, motor driver, steering wheel system and front wheel system interconnected via wires (represented as SbW system), a rotary encoder sensor, current sensor, potentiometer, and DC power supply. All equipment setups have been enumerated in Table 5, corresponding to the numbering in Figure 15.

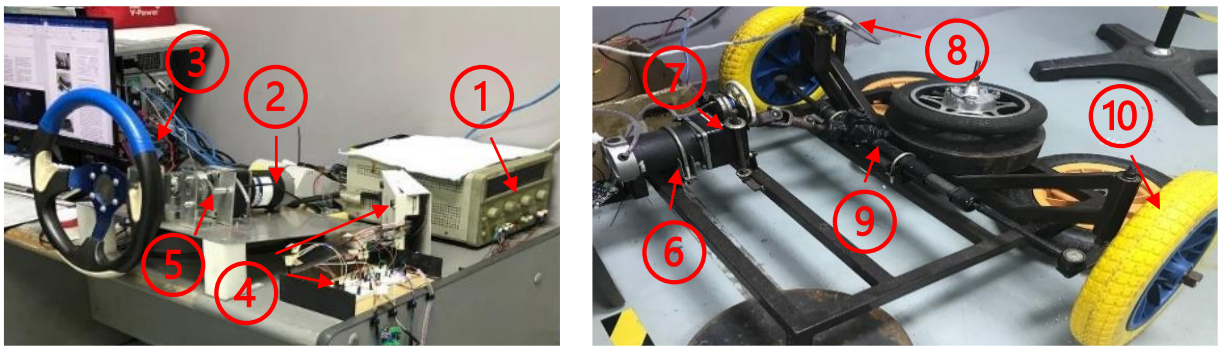

(a) (b)

Figure 15. Experiment of SbW test rig; (a) Steering wheel rig, (b) Front wheel rig

Table 5. SbW test rig equipment

No.	Equipment	No.	Value
1.	Laboratory DC power supply	6.	Front wheel DC motor
2.	Steering wheel DC motor	7.	Potentiometer
3.	Steering wheel	8.	Rotary encoder
4.	PCI-6221 DEQ and SCB-68 NI board	9.	Steering rack system
5.	Belt and pulley system integrated with potentiometer	10.	Front wheel

The signal inputs that will be running in the simulation and HiLS are step input, sinusoidal wave, square wave, and sawtooth wave. By obtaining the PID parameter from the Ziegler-Nichol's method, the simulation MATLAB Simulink and HiLS result for steering wheel angle (SWA) have been plotted and shown in Figure 16(a) to Figure 16(d) for PID-based controller in the steering wheel model.

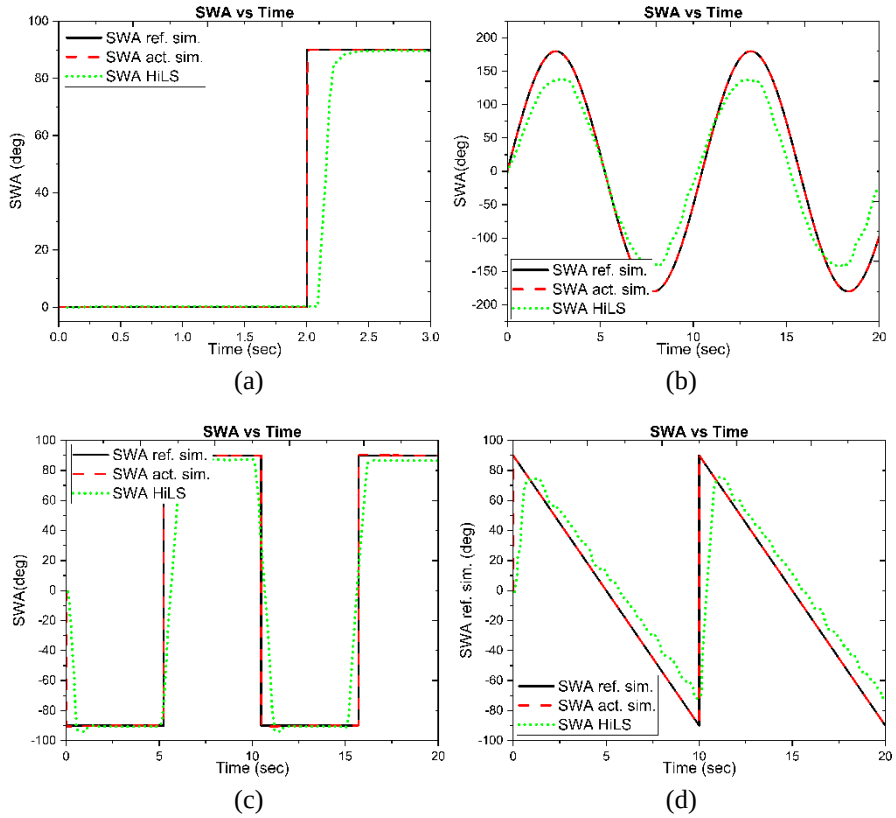

Figure 16. Signal response for SWA; (a) step input, (b) sinusoidal wave, (c) square wave and (d) sawtooth wave

As shown in Figure 16(a), the PID performance from MATLAB Simulink result indicated the settling time is about 2.03 seconds and the rise time is about 2.01 seconds, with no reported overshoot phenomenon during simulation. Meanwhile, the HiLS result demonstrated a settling time of about 2.42 seconds and a rise time of about 2.21 seconds with no observed overshoot phenomenon. The short settling time and rise time indicate the PID controller's ability to swiftly attain the desired target and promptly respond to input changes. From Figure 16(b) to Figure 16(d), the PID controller is

able to track the position of the sinusoidal, square and saw tooth wave input with a small deviation of magnitude. These findings collectively affirm the effectiveness of the PID controller in accurately tracking the steering wheel angle (SWA) input across both simulation and HiLS tests.

4.4 Position Tracking Front Wheel Model in SbW system

For the front wheel model (refer to Figure 14), the block diagram was designed based on equations (50) to (54) and executed in MATLAB Simulink environment. The same method as mentioned in Section 4.3, which is the HiLS test, was executed to validate the PID application of the front wheel model in the SbW system. By obtaining the PID parameter from the Ziegler-Nichol's method, the result for simulation and HiLS tests of tire steer angle (TSA) have been plotted in Figure 17(a) to Figure 17(d).

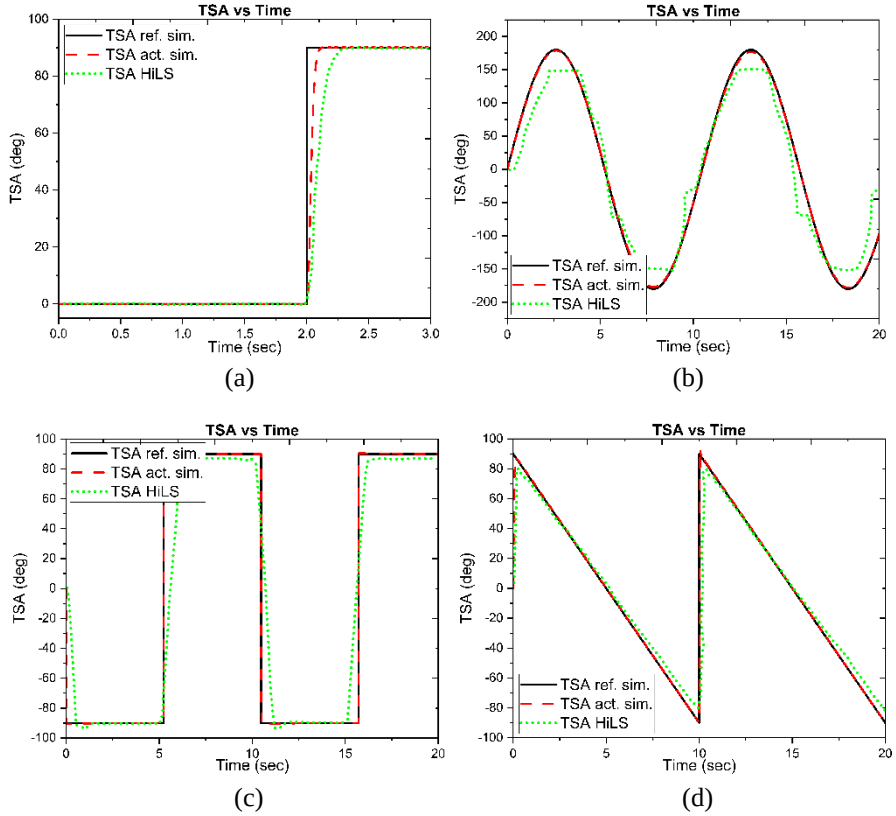

Figure 17. Signal response for TSA; (a) step input, (b) sinusoidal wave, (c) square wave and (d) sawtooth wave

From Figure 17(a), the PID performance is illustrated using MATLAB Simulink results, showcasing a settling time of about 2.12 seconds and the rise time of about 2.07 seconds, with no reported overshoot phenomenon. Meanwhile, the HiLS results demonstrate a settling time of around 2.27 seconds and a rise time of approximately 2.17 seconds, with no observed overshoot phenomenon. The PID controller's performance, as observed by its short settling time and rise time, shows its capability to quickly achieve the desired target input and respond faster to input changes. From Figure 17(b) to Figure 17(d), the PID controller adeptly tracks the sinusoidal, square and saw tooth wave input, displaying similar patterns and slighly different in magnitude. These findings show the application of the PID controller in the front wheel model is effective in tracking the position of the tire steer angle (TSA) input. The outcomes presented in Section 4.3 and Section 4.4 highlight the PID controller theoretically valid for tracking control of the SbW system.

5. IMPLEMENTATION OF PROPOSED STEER-BY-WIRE SYSTEM IN 14-DOF VEHICLE MODEL

The SbW model, as described in Section 4.0 was integrated with the 14-DOF vehicle dynamic model, and then simulated results were explained in this section. Figure 18 shows the overall block diagram of the integration of the SbW-14DOF model. The SbW model obtains the input from two (2) sources of the 14-DOF vehicle model, which are from steering wheel angle input, θ_{sw} and aligning moment, M_z. Then, the SbW model provided the deflection angle for both side of the tires (front left and front right), δ_{fl} and δ_{fr} that were utilized by the full (14-DOF) vehicle dynamic model. In order to verify this proposed model (SbW-14DOF model), it needs to be verified with the 14-DOF vehicle dynamic model that has been validated with the conventional full vehicle model available in CarSim software in Section 3.0 and then compare the simulation results. At the validation stage, two (2) vehicle dynamic tests, namely the DLC test and SSI test, were performed.

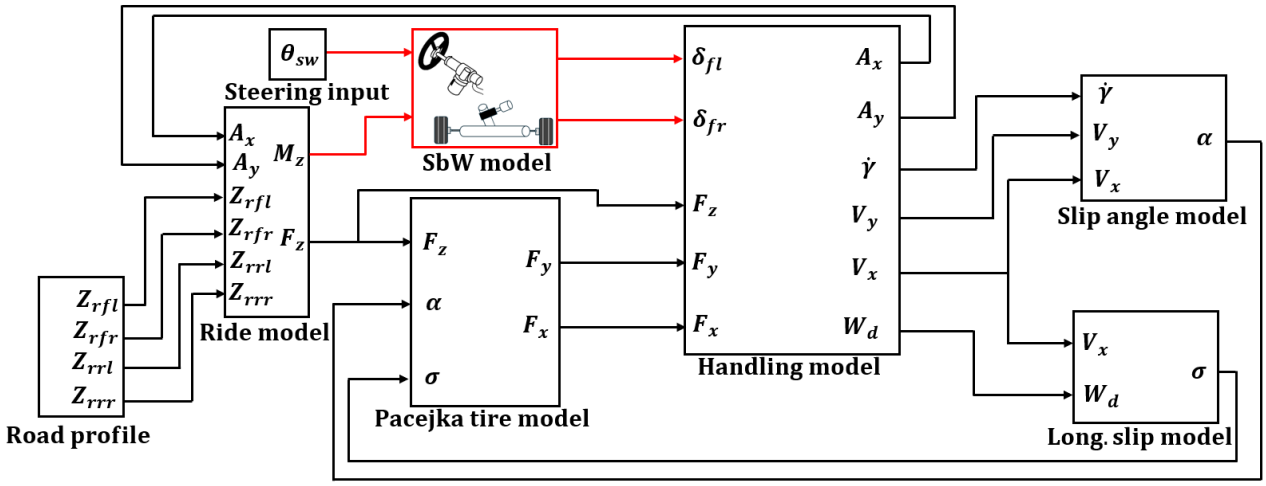

Figure 18. Implemented proposed SbW model in 14-DOF vehicle dynamic model

As a test method, the DLC test was conducted with a constant speed of 80 km/h and the SSI test was conducted with 60 km/h at 180°. The derivation of the output, specifically the deflection angle and slip angle of the front left tire, lateral acceleration, and yaw rate were presented. The steering wheel input for each test is depicted in Figures 15(a) and 15(b), as mentioned in Section 4.0. The results for the DLC test, illustrated in Figure 19(b) to Figure 19(d), exhibit a similar pattern but slight variations in magnitude. The RMS error percentage indicates approximately 0.02% for lateral acceleration, 0.10% for yaw rate and 0.02% for slip angle.

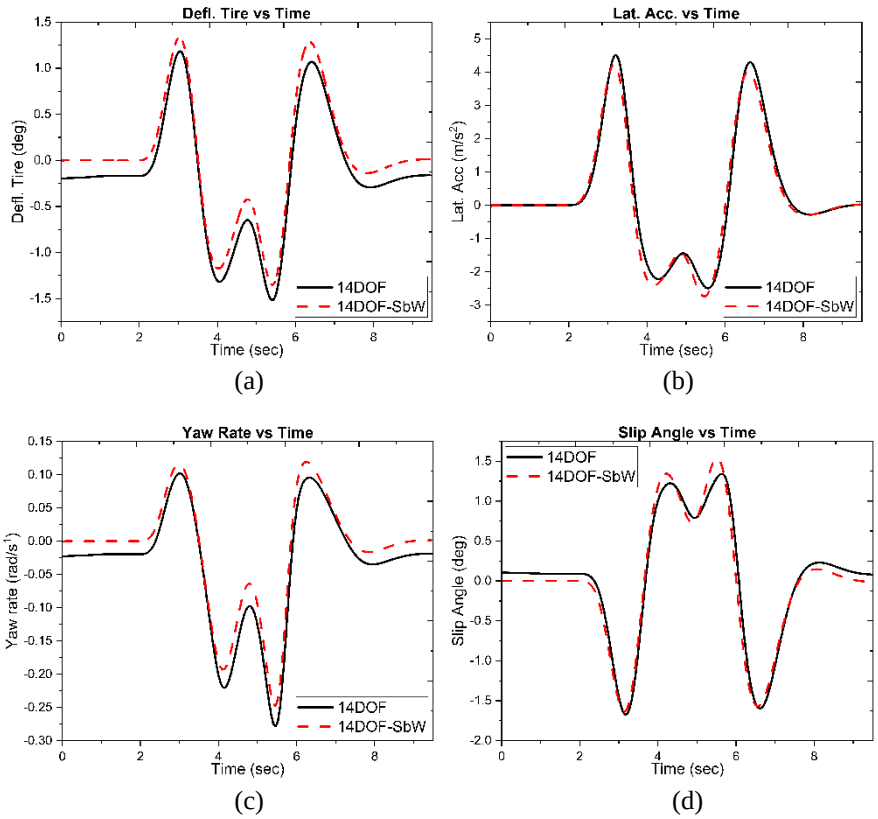

Figure 19. Vehicle dynamic characteristic for DLC test; (a) deflection angle of the front left tire, (b) lateral acceleration, (c) yaw rate and (d) slip angle of the front left tire

The SSI test results show that the SbW-14DOF model demonstrates acceptable deviation in pattern while maintaining consistent magnitude, as illustrated in Figure 20(b) to Figure 20(d). Based on the results, the RMS error percentage for lateral acceleration is 0.02%, the yaw rate is 0.01% and the slip angle is 0.01%, respectively. Despite the small RMS error percentage from both tests, it can be inferred that the SbW-14DOF model effectively follows the trends of the 14-DOF vehicle model with a conventional steering system. This error may be caused by the involvement of the non-linear hysteretic behavior inherent in the SbW model [65]–[66]. The small angle tracking error shown in Figure 19(a) and Figure 20(a) demonstrates that the SbW-14DOF model has good angle following characteristics and accurately reflects the dynamic characteristic of the vehicle.

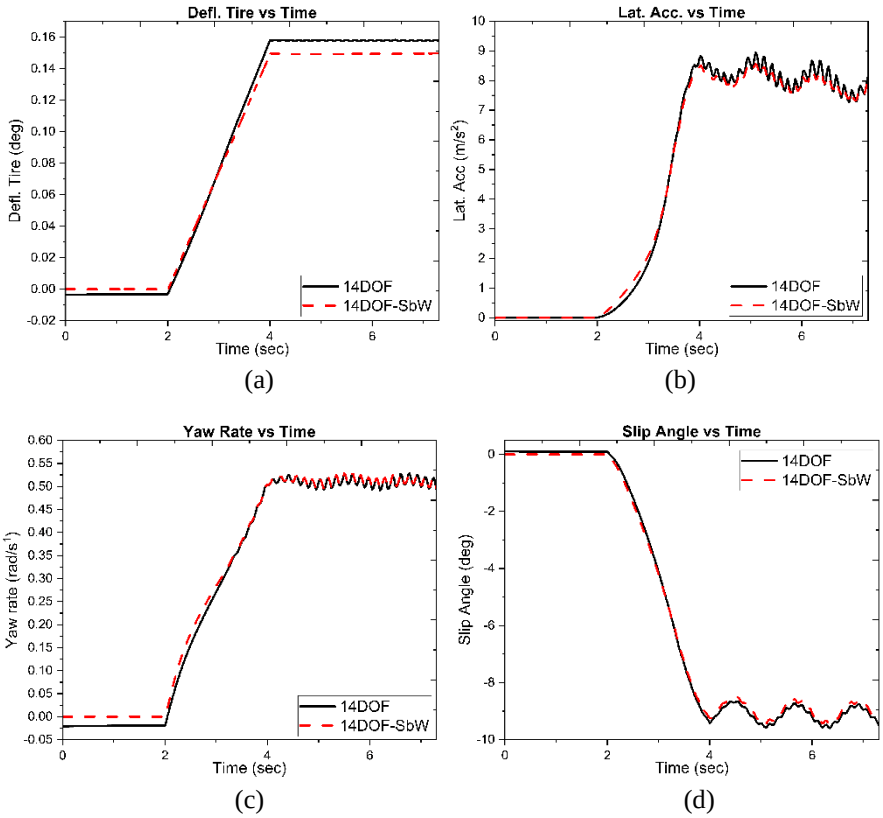

Figure 20. Vehicle dynamic characteristic for SSI test; (a) deflection angle of the front left tire, (b) lateral acceleration, (c) yaw rate and (d) slip angle of the front left tire

The SbW system that was developed initially mirrored conventional fixed steering ratios. However, integrating the Variable Steering Ratio (VSR) design into the SbW system it will improve the steering characteristic of a vehicle to a certain extent. This evolution not only meets the fundamental control requirements of the steering system but also elevates the driving experience to new levels of precision, adaptability and driver workload issues. In the next section, the introduction of the VSR control strategy will be explored, detailing its implementation and illustrating the tangible results it brings to the SbW model. Through this exploration, the transformative impact of the VSR control strategy on SbW systems becomes evident in the development of the steering system.

5.1 Variable Steering Ratio (VSR) Implemented in SbW-14DOF System

The variable steering ratio (VSR) incorporated into the steering tracking control strategy of the SbW system has enhanced the vehicle's steering characteristics to a certain degree and largely fulfilled the control requirements of the steering system. However, during the actual vehicle operation, the conditions are intricate, and numerous disruptive factors exist. Consequently, the active steering control strategy is introduced. Active steering control technology has gained widespread adoption in enhancing vehicle driving safety and handling stability. It effectively utilizes tire lateral forces without adjustments to driving or braking forces and executes superimposed steering interventions with greater accuracy and speed, thereby swiftly stabilizing the vehicle.

The steering ratio in a steering system generally represents the correlation between the steering wheel angle, θ_{sw}, and the front wheel angle, δ_{wheel}. By removing mechanical linkages, a SbW system allows for adjustable steering ratios, improving maneuverability at lower speeds and enhancing stability at higher speeds, thereby boosting overall vehicle handling performance. Currently, the traditional steering ratio typically relies on fixed steering gain. This design approach aims to lower the vehicle's complex characteristic impact on the user experience [67]. In this section, an adjustable steering gain approach is employed to design the dynamic steering ratio for routine driving using a VSR control strategy, with the goal of reducing driver effort, enhancing vehicle response, and improving steering stability.

The desired steering response, θ_{sw} is obtained from the 14-DOF vehicle dynamic model, which requires a target front wheel angle, δ_{wheel} . The VSR control strategy calculates δ_{wheel} based on vehicle speed and the steering actuation module adjusts the front wheel angle according to the constant steering ratio (CSR) value, i using driver/user input angle, θ_{sw}. The steering gain of a vehicle consists generally of two (2) factors: yaw rate factor and lateral acceleration factor. The yaw rate factor is defined as the yaw rate of the θ_{sw} ratios, whereas the lateral acceleration factor represents the y-axis acceleration to the θ_{sw} ratios. Given the interrelationship between yaw rate and lateral acceleration, the equation that was developed focuses solely on the yaw rate factor. The steering ratio of the SbW system is defined by equations (55) and (56) as follows:

$$G_{wr} = \frac{\dot{\gamma}}{\theta_{sw}} = \frac{\dot{\gamma}}{\delta_{wheel}(\beta i)} = f_{\beta}(V_x) \tag{55}$$

where G_{wr} represents the yaw rate factor and δ_{wheel} denotes the front wheel angle

Additionally, the steering ratio, i, is:

$$\beta i = \frac{\theta_{sw}}{\delta_{wheel}} \tag{56}$$

From equation (56), β represents the calibration coefficient of the steering ratio, which is calculated according to the control law. At low speeds, a smaller steering ratio is desirable to enhance handling and steering agility. Conversely, to enhance driving stability and safety at higher speeds, an improved steering ratio is necessary to reduce steering sensitivity. Due to mechanical constraints on the steering rack's range of motion, a lower limit on the steering ratio, β_{min} relative to vehicle speed is taken into account. Furthermore, an upper limit, β_{max} is implemented to prevent slow response during high-speed driving. Designing the steering ratio for different vehicle speed ranges requires careful consideration. At low speeds, the design should ensure the steering remains responsive and aligns with the driver's handling preferences. For moderate speeds, the focus should be on maintaining a consistent yaw rate factor. Meanwhile, at high speeds, it is important to manage steering sensitivity to ensure stability. This analysis leads to the presentation of the newly proposed VSR based on the National Highway Traffic Administration (NHTSA) speed category standard [68]. The newly proposed VSR is given by,

$$\beta = \begin{cases} \beta_{min}, V_x < 40\ kmh^{-1} \\ f_{\beta}(V_x), 40\ kmh^{-1} \leq V_x < 100\ kmh^{-1} \\ \beta_{max}, 100\ kmh^{-1} \leq V_x < 120\ kmh^{-1} \end{cases} \tag{57}$$

The above formula is the correlation between calibration coefficient β and vehicle speed V_x. The steering ratio design for low vehicle speeds aims to prioritize steering lightness and reduce driver effort. Conventional mechanical steering systems typically maintain a nearly constant steering ratio, requiring drivers to make 3 to 4 turns of the steering wheel. However, when making sharp turns, drivers must rapidly turn the steering wheel, increasing their steering workload. To address this, the steering ratio design considers drivers' habits at low speeds, aiming for ease of steering while avoiding excessively sensitive front wheel responses to steering wheel inputs. This is achieved by setting a minimum steering ratio, denoted as i_{min}. This setting is to ensure that the front wheel steering angle does not exceed the limit, δ_{fmax}, typically between 35°and 45°, which is at the maximum angle of the steering wheel, δ_{swmax}. In this study, δ_{swmax} is set as 810°, equivalent to 2.25 turns of the steering wheel. The derivation for i_{min} is determined as,

$$\begin{aligned} i_{min} &= \frac{\delta_{sw_{max}}}{\delta_{f_{max}}} \\ &= \frac{810}{45} = 18 \end{aligned} \tag{58}$$

If the current steering ratio, i_n falls below i_{min}, it is adjusted to i_{min}. The data for equation (58) are based on the data gathered from a real EV prototype at UTeM Laboratory. For vehicle speeds ranging from 40 - 100 km/h, the steering ratio is designed with the aim of achieving the optimal yaw rate factor. This ensures that the vehicle maintains a steady yaw rate within the desired range, which decreases as the speed of the vehicle increases. Typically, the yaw rate factor for an average driver falls between 0.16 and 0.37 s^{-1}. At higher vehicle speeds, categorized as 100 km/h and above, steering sensitivity becomes crucial. It quantifies the immediate change in lateral acceleration concerning the θ_{sw}, representing the incremental lateral acceleration produced by each degree of steering wheel rotation. This relationship can be expressed as follows:

$$S_s = \frac{100\Delta a_y}{\Delta \delta_{sw}} \tag{59}$$

Typically, steering sensitivities range from 0.9 to 1.4 g per 100 degrees [69]. If the vehicle's steering sensitivity surpasses 1.4 g per 100 degrees, it can lead to oversteering [70], necessitating a restriction on steering sensitivity. As mentioned in [71], for a speed of 100 km/h, the acceptable range of steering sensitivity for a vehicle is between 0.95 and 1.2 g per 100 degrees. Figure 21 depicts the steering ratio characteristics for the proposed VSR control strategy across the full speed range, from 0 to 120 km/h, encompassing both low and high vehicle speed categories.

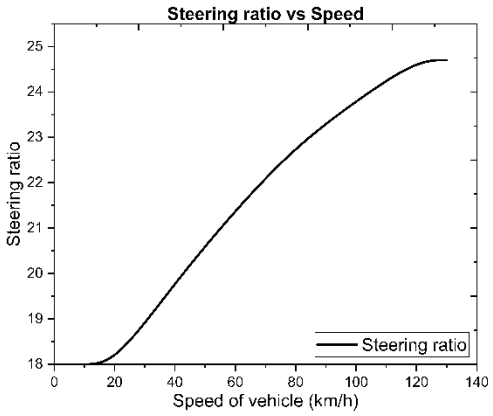

Figure 21. The dynamic steering ratio at different speeds of the vehicle

5.2 Simulation Analysis

By implementing the equation (55) to (57) into the SbW model, the SbW-14DOF model integrated with the VSR control strategy commenced operation. To verify the efficiency of the proposed VSR control strategy, a simulation was conducted using CarSim software and MATLAB Simulink on the DLC test. The SbW-14DOF integrated with the VSR controller is compared with the conventional steering vehicle, which maintains a constant steering ratio. A constant value of 18 was selected for the CSR of the conventional steering system. The DLC test was performed across three (3) speed categories: low, medium, and high-speed range. The efficacy of the VSR control strategy was particularly evident at low speeds, where drivers typically engage in parking maneuvers. In medium-speed scenarios, reflective of urban driving conditions, and high-speed scenarios, where rapid steering responses are crucial, the VSR's impact was further assessed. The DLC test series are at 30 km/h (low-speed), 80 km/h (medium-speed), and 120 km/h (high-speed).

From the DLC test, the results of low, middle and high vehicle speed categories have been plotted in Figure 22 to Figure 24, specifically on the yaw rate, lateral acceleration and slip angle of the tire. Based on simulation outcomes, it can be ensured that both the SbW steering vehicle and conventional steering vehicle can finish the DLC test. The SbW vehicle with a VSR control strategy has a better dynamic response. Figure 22 shows a marginal reduction in the vehicle's yaw rate at low speeds, which becomes significantly pronounced as the vehicle accelerates from middle to high speeds, indicating that the vehicle is stabilizing its motion. Moreover, the reduction in yaw rate gradually tapers off as the vehicle transitions from middle to high speeds. This concludes that the vehicle responds predictably to steering input and maintains better control, resulting in enhanced handling characteristics. Consistent with prior research by Liu et al. [72], the decrease in yaw rate observed in VSR applications evidently contributes to the enhanced steering stability of SbW vehicles. Notably, as highlighted in Wang et al. [73] research work, rapid changes in vehicle yaw rate may induce panic in drivers, leading to inappropriate steering actions and potentially causing accidents.

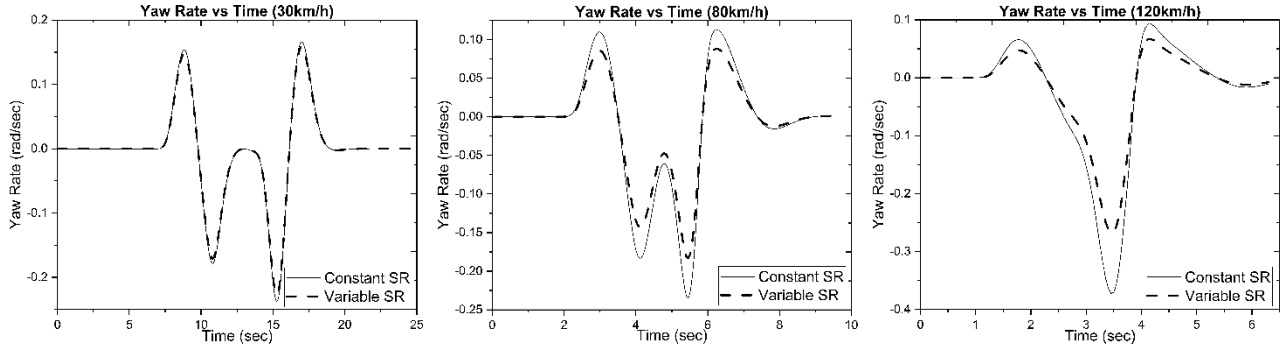

(a) (b) (c)

Figure 22. Yaw rate of low, middle and high vehicle speed varies with time

The application of the VSR strategy in SbW also improves lateral acceleration characteristics at each speed range, as demonstrated in Figure 23. Analysis of the results reveals a gradual decrease in lateral acceleration observed during the transition from low to high speeds. While the magnitude of improvement may appear modest, its significance lies in its impact on mitigating the risk of oversteer or understeer, both of which can precipitate loss of control and potential accidents. The decrease in lateral acceleration indicates the vehicle is making gentler turns or maneuvers, leading to an enhanced and more controlled ride. Correspondingly, aligning with findings from Wang et. al., [74], the observed decrease in lateral acceleration in VSR applications enhances driver safety and stability, enabling the driver to navigate maneuvers with greater confidence.

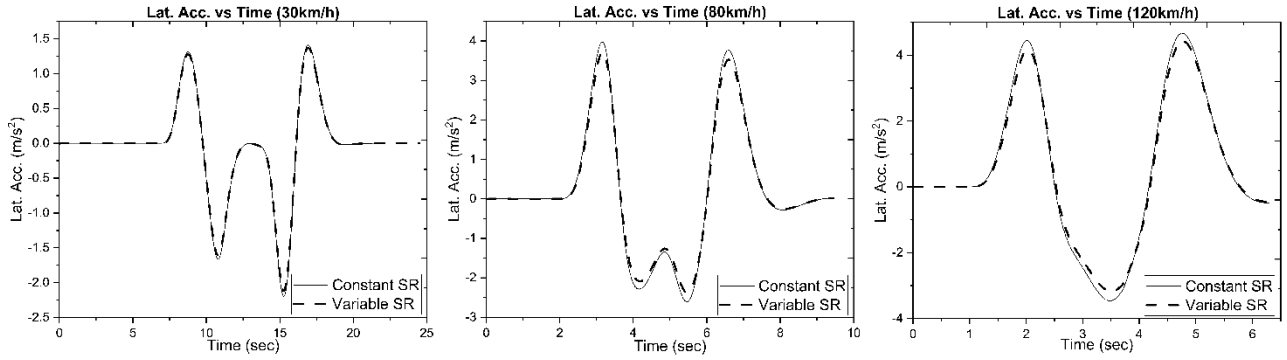

(a) (b) (c)

Figure 23. Lateral Acceleration of low, middle and high vehicle speed varies with time

Based on Figure 24, as the slip angle decreases in SbW vehicles compared to conventional steering vehicles, it demonstrates the VSR controller can alleviate the driver's steering workload, leading to enhanced comfort and ease while maneuvering for the driver, especially during cornering and tight turns. This is supported by research from Fuse and Fujimoto [75], which indicates that employing a VSR strategy reduces tire slip angles and steering angles by approximately 20%, thereby enhancing vehicle maneuverability. Additionally, insights from Yoshino and Nozaki [76] highlighted that the reduction in vehicle slip angle through the application of the VSR controller correlates with decreased tire slip and improved traction, ultimately resulting in reduced driver steering workload. Hence, drawing from previous research findings, it can be concluded that the implementation of the VSR strategy leads to an enhancement in vehicle dynamic characteristics.

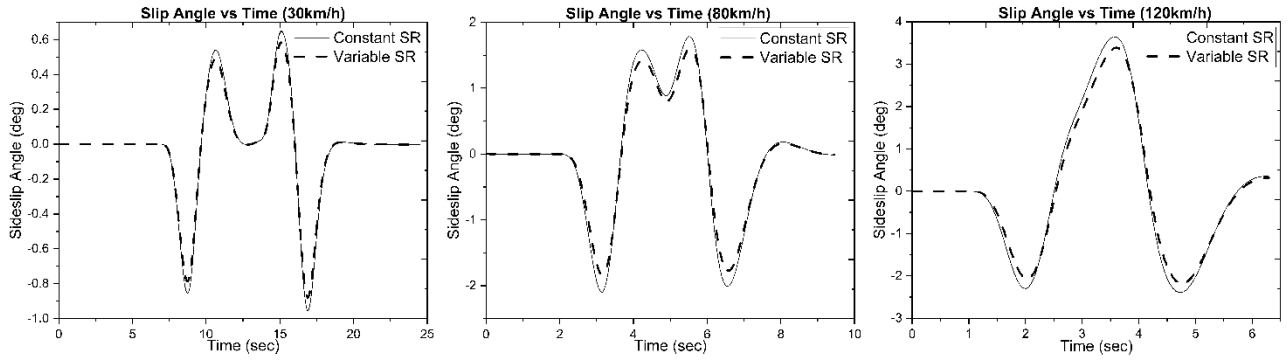

(a) (b) (c)

Figure 24. Slip angle of low, middle and high vehicle speed varies with time

Figure 25 records the results of the yaw rate factor and steering sensitivity. It is observed for low to middle vehicle speed categories, the values range from 0.22 to 0.35 seconds^{-1}. The range of the yaw rate factor is deemed acceptable compared to the value mentioned by [46, 77]. However, for high vehicle speed categories, the critical element that requires review is steering sensitivity, which, according to [46, 77], ranges from 0.9 to 1.4 g. In this study, the steering sensitivity ranges obtained are from 1.01 to 1.11 g for vehicle speeds between 100 km/h and 120 km/h. Therefore, integrating the VSR control strategy into the SbW system has significantly enhanced the steering stability of SbW vehicles while simultaneously alleviating the driver's workload. These findings are further strengthened by integrating the proposed SbW system with a comprehensive 14-DOF vehicle dynamic model in simulation environments.

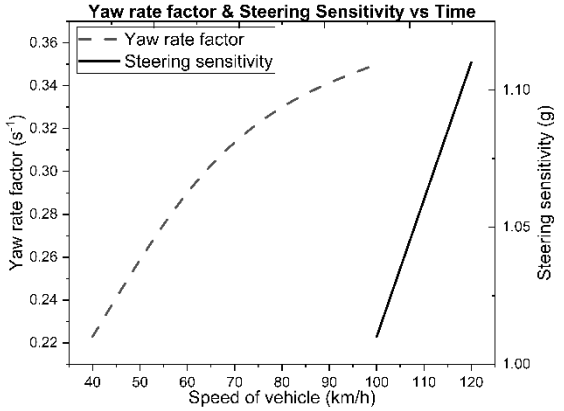

Figure 25. Yaw rate factor and steering sensitivity vary with the speed of vehicle

6. CONCLUSION

In this research work, a comprehensive 14-DOF vehicle dynamic model was developed using MATLAB Simulink. The accuracy of this model was assessed through rigorous validation against CarSim software to ensure the 14-DOF closely mirrors the real-world vehicle dynamic. The validation stage involves two (2) dynamic tests complying with ISO standards: a DLC test at 80 km/h and an SSI test at 60 km/h with a 180° turn. Results revealed that while some slight deviations in root mean square (RMS) percentage errors were presented, the 14-DOF vehicle dynamic model effectively encapsulated the essence of real-world vehicle dynamics. Building upon this foundation, the study progressed to develop and validate a Steer-by-Wire (SbW) model in both simulation and HiLS environments. The SbW system, employing a PID-based controller, was meticulously developed within MATLAB Simulink. CarSim output and MATLAB Simulink results were compared in validation testing. To further bolster confidence in the PID controller's efficacy for position tracking, the SbW system underwent testing in a HiLS setup facilitated by the development of an SbW test rig. Encouragingly, the results demonstrated the PID controller's adeptness in achieving precise position tracking within the SbW system. Recognizing the importance of integrating dynamic vehicle behavior with SbW functionality, the study constructed a unified SbW-14DOF model within MATLAB Simulink. This amalgamated model thorough validation, with SSI test and DLC tests selected to verify its dynamic characteristics. Comparisons with the 14-DOF vehicle dynamic model (consists of a conventional steering system) demonstrate that the SbW-14DOF model faithfully mirrored its behavior, albeit with minor RMS percentage errors. Continuing the trajectory of advancement, the study delved into the development of a novel Variable Steering Ratio (VSR) strategy. This strategy aimed to alleviate driver workload on the steering wheel while enhancing vehicle stability. Through implementation within the 14-DOF vehicle dynamic model, it was observed that the PID control strategy adeptly tracked trajectories, thus validating the efficacy of the proposed VSR strategy. For future works, it is imperative to explore further enhancements to the SbW system, particularly focusing on bolstering its robustness. Additionally, there is a pressing need to develop the VSR control strategy within the hardware system and subject it to rigorous testing through comparative experiments conducted in HiLS tests. Besides that, the proposed SbW system needs to be implemented into real-world applications, with particular emphasis on testing in authentic driving environments and also considering the value added from human-vehicle interaction.

ACKNOWLEDGEMENT

The authors would like to express their gratitude to the Universiti Teknikal Malaysia Melaka (UTeM) for providing feasible research facilities for this study. Additionally, the first author would also like to thank the Malaysian Ministry of Higher Education (MOHE) and Universiti Tun Hussein Onn Malaysia (UTHM) for granting the scholarships to pursue the PhD program studies.

CONFLICT OF INTEREST

All author(s) have agreed with the contents of the manuscript, and there are no financial or non-financial interests to report.

AUTHOR CONTRIBUTION

M. A. Azizul (Methodology, Data Curation; Writing – original draft)

F. Ahmad (Conceptualization; Model Verification; Supervision)

J. Karjanto (Funding acquisition; Visualisation; Supervision)

M. H. Che Hasan (Formal analysis; Writing - review & editing)

S. Sulaiman (Visualisation; Data Interpretation)

REFERENCES

[1] G. Perozzi, J.J. Rath, C. Sentouh, J. Floris, and J.C. Popieul, "Lateral shared sliding mode control for lane keeping assist system in steer-by-wire vehicles: Theory and experiments," *IEEE Transactions Intelligent Vehicles*, vol. 8, no. 4, pp. 3073–3082, 2023.

[2] M. Irmer, R. Degen, A. Nubgen, K. Thomas, H. Henrichfreise, and M. Ruschitzka, "Development and analysis of a detail model for steer-by-wire systems," *IEEE Access*, vol. 11, pp. 7229–7236, 2023.

[3] G. Chen, M. Hua, W. Liu, J. Wang, S. Song, and C. Liu, "Planning and tracking control of full drive-by-wire electric vehicles in unstructured scenario," *Proceedings of the Institution of mechanical Engineering, Part D: Journal of Automotive Engineering*, p. 09544070231195233, 2023.

[4] X. Wu and W. Li, "Variable steering ratio control of steer-by-wire vehicle to improve handling performance," *Proceedings of the Institution of Mechanical Engineering, Part D: Journal of Automotive Engineering*, vol. 234, no. 2–3, pp. 774–782, 2020.

[5] A. Norouzi, M. Masoumi, A. Barari, and S. Farrokhpour Sani, "Lateral control of an autonomous vehicle using integrated backstepping and sliding mode controller," *Proceedings of the Institution of Mechanical Engineering, Part K: Journal Multi-body Dynamics*, vol. 233, no. 1, pp. 141–151, 2019.

[6] A. Li, C. Niu, S. Li, X. Huang, C. Xu, and G. Liu, "Research on intelligent vehicle trajectory planning and control based on an improved terminal sliding mode," *Applied Sciences*, vol. 12, no. 5, pp. 2446, 2022.

[7] G. Perozzi, M.R. Oudainia, C. Sentouh, J.C. Popieul, and J.J. Rath, "Driver assisted lane keeping with conflict management using robust sliding mode controller," *Sensors*, vol. 23, no. 1, p. 4, 2023.

[8] K. Kim, J. Lee, M. Kim, and K. Yi, "Adaptive sliding mode control of rack position tracking system for steer-by-wire vehicles," *IEEE Access*, vol. 8, pp. 163483–163550, 2020.

[9] S. Chen and H. Chen, "MPC-based path tracking with PID speed control for autonomous vehicles," in *IOP Conference Series: Material Science and Engineering*, 2020, vol. 892, no. 1, pp. 3702-3720.

[10] W. Wang, J. Liang, C. Pan, and L. Chen, "Hierarchical CNNPID based active steering control method for intelligent vehicle facing emergency lane-changing," *Chinese Journal of Mechanical Engineering (English Ed)*, vol. 36, no. 1, p. 100, 2023.

[11] R. Zhao, W. Deng, B. Ren, and J. Ding, "Modeling on steering feedback torque based on data-driven method," *IEEE/ASME Transactions on Mechatronics*, vol. 27, no. 5, pp. 2775–2785, 2022.

[12] C. Huang, F. Naghdy, and H. Du, "Sliding mode predictive tracking control for uncertain steer-by-wire system," *Control Engineering Practice*, vol. 85, pp. 194–205, 2019.

[13] R. Li, Y. Li, S. E. Li, C. Zhang, E. Burdet, and B. Cheng, "Indirect shared control for cooperative driving between driver and automation in steer-by-wire vehicles," *IEEE Transactions on Intelligent Transportation System*, vol. 22, no. 12, pp. 7826–7836, 2021.

[14] C. Bao, J. Feng, J. Wu, S. Liu, G. Xu, and H. Xu, "Model predictive control of steering torque in shared driving of autonomous vehicles," *Science Progress*, vol. 103, no. 3, p. 0036850420950138, 2020.

[15] Z. Sun, J. Zheng, Z. Man, and J. Jin, "Discrete-time iterative learning control for vehicle steer-by-wire systems," in *2014 9th IEEE Conference on Industrial Electronics and Applications*, Hangzhou, China, 2014 June 9-11, pp. 462–467.

[16] M.Z. Mohd Tumari, M.S. Saealal, W.N. Abd Rashid, S. Saat, and M.A. Mohd Nasir, "The vehicle steer by wire control system by implementing PID controller," *Journal Telecommunication, Electronic and Computer Engineering*, vol. 9, pp. 43–47, 2017.

[17] M.Z. Mohd Tumari, M.A. Mohd Nasir, S. Saat, and A.S.R. Abd Subki, "The control schemes of vehicle steer by wire system by using fuzzy logic and PID controller," *Research Journal of Applied Sciences*, vol. 13, no. 2, pp. 137–145, 2019.

[18] F. Hunaini, F. Nugroho, P. Suwandono, and G. Subiyakto, "The cascade optimal control of steer by wire system using hardware in the loop simulations," *International Journal of Power Electronics and Drive Systems*, vol. 13, no. 2, pp. 764–772, 2022.

[19] R. Gonschorek and T. Bertram, "Robust two-degrees of freedom linear quadratic gaussian position control for the front axle actuator of a steer-by-wire system," *Forsch. im Ingenieurwesen/Engineering Res.*, vol. 87, no. 2, pp. 697–710, 2023.

[20] X. Wu, M. Zhang, and M. Xu, "Active tracking control for steer-by-wire system with disturbance observer," *IEEE Transactions on Vehicular Technology*, vol. 68, no. 6, pp. 5483–5493, 2019.

[21] D.S. Cheon and K.H. Nam, "Steering torque control using variable impedance models for a steer-by-wire system," *International Journal Automotive Technology*, vol. 18, no. 2, pp. 263–270, 2017.

[22] N. El Fezazi, E.H. Tissir, F. El Haoussi, F.A. Bender, and A.R. Husain, "Controller synthesis for steer-by-wire system performance in vehicle," *Iran Journal Science Technology Transactions of Electrical Engineering*, vol. 43, no. 4, pp. 813–825, 2019.

[23] H. Zhou, A. Pang, J. Yang, and Z. He, "Structured H∞ control of an electric power steering system," *Complexity*, vol. 2020, 2020.

[24] S. Do Na, J.S. Jang, K.S. Kim, and W.S. Yoo, "Dynamic vehicle model for handling performance using experimental data," *Advances in Mechanical Engineering*, vol. 7, no. 11, pp. 1–12, 2015.

[25] R.N. Jazar. Vehicle Dynamics: Theory and Application. 3rd ed. Boston, MA: Springer US, 2008.

[26] R. Rajamani. Vehicle Dynamics and Control (Mechanical Engineering Series). 2nd ed. Boston, MA: Springer US, 2012.

[27] F. Heinrich, J. Kaste, S.G. Kabil, M. Sanne, F. Küçükaym R. Henze, *et al.*, "Methods for modeling the steering wheel torque of a steer-by-wire vehicle," *Automotive and Engine Technology*, vol. 7, no. 1–2, pp. 53–64, 2022.

[28] S. M. Sahboun and A. A. A. Emhemed, "Controller design for steer-by-wire system," *Journal of Mechatronics and Robotics*, vol. 6, no. 1, pp. 1–6, 2022.

[29] J. Tian, G. Tan, X. Pan, M. Cai, C. Huang, and Y. Yan, "Research on road sense simulation and stability control of SBW system," in *2021 China Automation Congress (CAC) 2021*, Beijing, China, October 22-24 2021, pp. 4065–4070.

[30] S. C. Zou and W. Z. Zhao, "Synchronization and stability control of dual-motor intelligent steer-by-wire vehicle," *Mechanical Systems and Signal Processing*, vol. 145, p. 106925, 2020.

[31] H. Hwang, H. Choi, and K. Nam, "Practical synchronous steering angle control of a dual-motor driving steer-by-wire system," *IEEE Access*, vol. 7, pp. 133100–133110, 2019.

[32] L. De Novellis, A. Sorniotti, P. Gruber, and A. Pennycott, "Comparison of Feedback Control Techniques for Torque-Vectoring Control of Fully Electric Vehicles," *IEEE Transactions on Vehicular Technology*, vol. 63, no. 8, pp. 3612–3623, 2014.

[33] S. S. Husain, M. Q. Kadhim, A. S. M. Al-Obaidi, A. F. Hasan, A. J. Humaidi, and D. N. Al Husaeni, "Design of robust control for vehicle steer-by-wire system," *Indonesian Journal of Science and Technology*, vol. 8, no. 2, pp. 197–216, 2023.

[34] A. Reda, A. Bouzid, and J. Vásárhelyi, "Model predictive control for automated vehicle steering," *Acta Polytechnica Hungarica*, vol. 17, no. 7, pp. 163–182, 2020.

[35] D. Cheon, K. Nam, and S. Oh, "Design and robust control of a precise torque controllable steering module for steer-by-wire systems," *IEEE Transactions on Industrial Electronics*, vol. 69, no. 12, pp. 13245–13254, 2022.

[36] Y. Zhen, Z. Wang, J. Liu, T. Guan, Y. Zhang, M. Wang, et al., "Control strategy and simulation verification of hardware-in-the-loop system of automotive steering device," in *IOP Conference Series: Material Sciences and Engineering*, 2020 vol. 892, no. 1, p. 012048.

[37] F. Alfatti, M. Montani, T. Favilli, C. Annicchiarico, L. Berzi, M. Pierini, et al., "Implementation and performances evaluation of advanced automotive lateral stability controls on a real-time hardware in the loop driving simulator," *Applied Sciences*, vol. 13, no. 11, p. 6592, 2023.

[38] H. Efheij, A. Albagul, and N.A. Albraiki, "Comparison of model predictive control and PID controller in real time process control system," in *19th International Conference on Sciences and Technology of Automatic Control Computer Engineering (STA)*, Sousse, Tunisia, May 24-26 2019, pp. 64–69.

[39] F.X. Xu, X.H. Liu, W. Chen, C. Zhou, and B.W. Cao, "Fractional order PID control for steer-by-wire system of emergency rescue vehicle based on genetic algorithm," *Journal of Central South University*, vol. 26, no. 9, pp. 2340–2353, 2019.

[40] L. He, F. Li, C. Guo, B. Gao, J. Lu, and Q. Shi, "An adaptive PI controller by particle swarm optimization for angle tracking of steer-by-wire," *IEEE/ASME Transactions on Mechatronics*, vol. 27, no. 5, pp. 3830–3840, 2022.

[41] C. Huang, L. Li, and X. Wang, "Comparative study of two types of control loops aiming at trajectory tracking of a steer-by-wire system with coulomb friction," *Proceedings of the Institution of Mechanical Engineers, Part D: Journal of Automobile Engineering*, vol. 235, no. 1, pp. 16–31, 2021.

[42] K. Li, "PID tuning for optimal closed-loop performance with specified gain and phase margins," *IEEE Transactions on Control Systems Technology*, vol. 21, no. 3, pp. 1024–1030, 2013.

[43] P. Mercader, K.J. Åström, A. Banos, and T. Hägglund, "Robust PID design based on QFT and convex-concave optimization," *IEEE Transactions on Control Systems Technology*, vol. 25, no. 2, pp. 441–452, 2017.

[44] Y. Pan, X. Li, and H. Yu, "Efficient PID tracking control of robotic manipulators driven by compliant actuators," *IEEE Transactions on Control Systems Technology*, vol. 27, no. 2, pp. 915–922, 2019.

[45] P. Phetnok, A. Lonklang, and S. Tantrairatn, "Implementation of Steering-by-Wire Control System for Electric Golf Cart," in *2019 5th International Conference Control, Automation and Robotics (ICCAR)*, Beijing, China, April 19-22, 2019, pp. 373–376.

[46] Y. Wu, L. Wang, and F. Li, "Research on variable steering ratio control strategy of steer-by-wire system," *SAE Technical Paper*, no. 2018-01-1583, 2018.

[47] H. Yang, W. Liu, L. Chen, and F. Yu, "An adaptive hierarchical control approach of vehicle handling stability improvement based on steer-by-wire systems," *Mechatronics*, vol. 77, p. 102583, 2021.

[48] M.A. Abdullah, M.R. Ridzuan, F. Ahmad, J.F. Mohamed, and M. Ibrahim, "Vehicle active suspension control using multi-order PID approach," *Journal of Advance Manufacturing Technology*, vol. 11, no. 1, pp. 1–14, 2017.

[49] F. Ahmad, S.A. Mazlan, H. Zamzuri, H. Jamaluddin, K. Hudha, and M. Short, "Modelling and validation of the vehicle longitudinal model," *International Journal of Automotive and Mechanical Engineering*, vol. 10, no. 1, pp. 2042–2056, 2014.

[50] M. Soomro, M. K. Hassan, and F. Ahmad, "Modelling and validation of an electronic wedge brake system with realistic quarter car model for anti-lock braking system design," *International Journal of Integrated Engineering*, vol. 11, no. 4, pp. 70–80, 2019.

[51] S. Sulaiman, P. Mohd Samin, H. Jamaluddin, R. Abd Rahman, and M.S. Burhaumudin, "Modeling and validation of 7-DOF ride model for heavy vehicle," in *International Conference on Automotive, Mechanical and Material Engineering*, Penang, Malaysia, May 19-20 2012, pp. 109–112.

[52] M.R. Stone and M.A. Demetriou, "Modeling and simulation of vehicle ride and handling performance," in *Proceedings of the 2000 IEEE International Symposium on Intelligent Control. Held jointly with the 8th IEEE Mediterranean Conference on Control and Automation (Cat. No.00CH37147)*, Patras, Greece, July 19-20 2000, pp. 85–90.

[53] E. Bakker, L. Nyborg, and H.B. Pacejka, "Tyre modelling for use in vehicle dynamics studies," *SAE Transactions*, vol. 96, pp. 190-204, 1987.

[54] K. Bharat Singh and S. Sivaramakrishnan, "Extended Pacejka Tire Model for Enhanced Vehicle Stability Control," arXiv [Online], May 28 2023. Available: https://arxiv.org/abs/2305.18422

[55] P. Shi, Q. Zhao, R. Zhang, and L. Ye, "The simulation of tire dynamic performance based on magic formula," in *Proceedings of the 2017 2nd International Conference on Automation, Mechanical Control and Computational Engineering (AMCCE 2017)*, Beijing, China, March 25-26 2017, pp. 699–703.

[56] V.R. Aparow, K. Hudha, M.M.H. Megat Ahmad, and H. Jamaluddin, "Development and verification of a 9- DOF armored vehicle model in the lateral and longitudinal directions," *Jurnal Teknologi*, vol. 78, no. 6, pp. 117–137, 2016.

[57] S. Boyle, "Pacejka magic formula tire model parser," in *2019 International Conference on Computational Science and Computer Intelligence (CSCI)*, Las Vegas, USA, December 5-7 2019, pp. 517–518.

[58] K. H. Ali and F. A. A. Majeed, "Improve roll dynamic response of road vehicle to step steer input using semi-active PID suspension controller," *International Journal of Computer Applications*, vol. 161, no. 12, pp. 8–14, 2017.

[59] P. Grabski, M. Jaśkiewicz, R Jurecki, D Kurczyński, P Łagowski, T.L. Stańczyk, et al., "Lateral acceleration tests during circular driving maneuvers and double lane change," in *IOP Conference Series: Materials Science and Engineering*, 2022, vol. 1247, no. 1, p. 012009.

[60] I.-M. Bîndac, S. Bradley, P. Roșca, C. Pupăză, and T. Giurgiu, "Theoretical and experimental research on the double lane change maneuver," in *10th edition of the International Multidisciplinary Symposium "UNIVERSITARIA SIMPRO 2022":*

Quality and Innovation in Education, Research and Industry – the Success Triangle for a Sustainable Economic, Social and Environmental Development, Romania, October 27-29 2022, vol. 373, p. 00054.

[61] A. Udas, "Road Variability and Its Effect on Vehicle Dynamics Simulation," Master of Science, University of Iowa, United States, 2011.

[62] D. Toffin, G. Reymond, A. Kemeny, and J. Droulez, "Influence of steering wheel torque feedback in a dynamic driving simulator," in *DSC North America 2003 Proceedings*, Michigan, United States, October 8-10 2003, vol. 2003.

[63] S. Achyuthan and N.K. Prakash, "Modelling of a steer-by-wire system with force feedback and active steering," in *2017 International Conference on Intelligent Computing and Control Systems (ICICCS)*, Madurai, India, June 15-16 2017, pp. 676–680.

[64] S. Ancha, A. Baviskar, J.R. Wagner, and D.M. Dawson, "Ground vehicle steering systems: modelling, control, and analysis of hydraulic, electric and steer-by-wire configurations," *International Journal of Vehicle Design*, vol. 44, no. 1–2, pp. 188–208, 2007.

[65] A. Kirli and M. S. Arslan, "Optimization of parameters in the hysteresis-based steering feel model for steer-by-wire systems," *IFAC-PapersOnLine*, vol. 49, no. 3, pp. 129–134, 2016.

[66] M. S. Arslan, "A hysteresis-based steering feel model for steer-by-wire systems," *Mathematical Problems in Engineering*, vol. 1, p. 2313529, 2017.

[67] H. Zheng, S. Ma, and X. Na, "Design of a variable steering ratio for steer-by-wire vehicle with a joystick," *Advances in Mechanical Engineering*, vol. 9, no. 11, p.1687814017730753., 2017.

[68] C. Becker, J. Brewer, D. Arthur, and F. Attioui, "Functional safety assessment of a generic steer-by-wire steering system with active steering and four-wheel steering features," National Highway Traffic Safety Administration [Online], August 1 2018. Available: https://rosap.ntl.bts.gov/view/dot/37208

[69] D.H. Weir and R. J. Dimarco, "Correlation and evaluation of driver/vehicle directional handling data," *SAE Technical Paper*, no. 780010, 1978.

[70] J. Tajima, N. Yuhara, S. Sano, and S. Takimoto, "Effects of steering system characteristics on control performance from the viewpoint of steer-by-wire system design," *SAE Technical Paper*, no. 1999-01-0821, 1999.

[71] S.A. Millsap and E.H. Law, "Handling enhancement due to an automotive variable ratio electric power steering system using model reference robust tracking control," *SAE Technical Paper*, no. 960931, 1996.

[72] S. Liu, Y. Zhu, and X. Ji, "Research on design of variable gear ratio of steer-by-wire system and comprehensive feedback control of front wheel angle," in *2021 China Automation Congress (CAC)*, Beijing, China, October 22-24 2021, pp. 1898–1903.

[73] R. Wang, H. Zhang, and J. Wang, "Linear parameter-varying controller design for four-wheel independently actuated electric ground vehicles with active steering systems," *IEEE Transactions on Control Systems Technology*, vol. 22, no. 4, pp. 1281–1296, 2014.

[74] J. Wang, X. Zhou, X. Chen, Z. Wang, P. Wang, and E. Liu, "Development of HIL - real vehicle dual steering wheel test platform for automotive SBW system based on variable transmission ratio control," in *International Conference on Electric Vehicle and Vehicle Engineering (CEVVE 2023)*, Shenzhen, China, November 10-12 2023, vol. 2023, no. 26, pp. 88–98.

[75] H. Fuse and H. Fujimoto, "Fundamental study on driving force control method for independent-four-wheel-drive electric vehicle considering tire slip angle," in *IECON 2018 - 44th Annual Conference IEEE Industrial Electronics Society*, DC, USA, October 21-23 2018, vol. 1, no. 3, pp. 2062–2067.

[76] T. Yoshino and H. Nozaki, "Variable gear ratio control using vehicle body slip angle," *Engineering*, vol. 6, no. 8, pp. 439–448, 2014.

[77] F. Li, L. Wang, C. Liao, and Y. Wu, "Active steering control strategy of steer-by-wire system based on variable steering ratio," in *IEEE Conference and Expo Transportation Electrification Asia-Pacific (ITEC Asia-Pacific)*, Beijing, China, August 31 - September 3 2014, pp. 1–5.